

Neuronal and astroglial monocarboxylate transporters play key but distinct roles in hippocampus-dependent learning and memory formation

Citlalli Netzahualcoyotzi^a and Luc Pellerin^{a,b,1}

^aDepartment of Physiology, University of Lausanne, 7 Rue du Bugnon, 1005 Lausanne, Switzerland. ^bCentre de Résonance Magnétique des Systèmes Biologiques, UMR 5536, CNRS/Université de Bordeaux, 146 rue Léo Saignat, Bordeaux 33076, France.

Citlalli Netzahualcoyotzi's email address : citlalli.netza@unil.ch

Address correspondence to :

Prof. Luc Pellerin

INSERM U1082

2 Rue de la Milétrie

86021 Poitiers Cedex

France

Email: luc.pellerin@univ-poitiers.fr

Tel: +33 5 49 44 47 79

¹Present affiliation: INSERM U1082, Université de Poitiers, 86021 Poitiers cedex, France.

luc.pellerin@univ-poitiers.fr

ABSTRACT

Brain lactate formation, intercellular exchange and utilization has been implicated in memory formation. However, the individual role of either neuronal or astroglial monocarboxylate transporters for the acquisition and consolidation of information remains incomplete. Using novel transgenic mice and a viral vector approach to decrease the expression of each transporter in a cell-specific manner within the dorsal hippocampus, we show that both neuronal MCT2 and astroglial MCT4 are required for spatial information acquisition and retention (at 24 hours post-training) in distinct hippocampus-dependent tasks. Intracerebral infusion of lactate rescued spatial learning in mice with reduced levels of astroglial MCT4 but not of neuronal MCT2, suggesting that lactate transfer from astrocytes and utilization in neurons contribute to hippocampal-dependent learning. In contrast, only neuronal MCT2 was shown to be required for long-term (7 days post training) memory formation. Interestingly, reduced MCT2 expression levels in mature neurons result in a heterologous effect as it blunts hippocampal neurogenesis associated with memory consolidation. These results suggest important but distinct contributions of both neuronal MCT2 and astroglial MCT4 in learning and memory processes, going beyond a simple passive role as alternative energy substrate suppliers or in waste product disposal.

1. Introduction

In the central nervous system, lactate was long considered as a waste product and its accumulation a sign of tissue suffering. However, lactate is recognized now as a preferred substrate for neuronal oxidative metabolism (Bouzier-Sore et al. 2006), and is also crucial for the metabolic coupling between neurons and astrocytes driven by glutamate neurotransmission (González-Gutiérrez et al., 2020; Pellerin & Magistretti, 1994). Furthermore, lactate emerged as a potential neuroprotective agent in pathologies such as neonatal hypoxic-ischemic encephalopathy (Roumes et al., 2020), adult stroke (Castillo et al. 2015) or traumatic brain injury (Quintard et al., 2016). In parallel, lactate can act as a signaling molecule in the central nervous system as it can prompt various key activities (Brooks et al., 2018, Magistretti and Allaman, 2018). Thus, it can contribute to the redox status regulation and induces changes in gene expression (El Hayek et al., 2019; Margineanu et al., 2018; Yang et al., 2014). In addition, lactate can participate to cell-cell signaling, acting as a direct agonist of the hydroxycarboxylic acid receptor 1 (HCAR1) (Lauritzen et al., 2014; Morland et al., 2017). Regarding its importance for cognition, it is also known that correct production/synthesis of lactate is determinant to perform some behavioral tasks (Gibb et al., 2006; Harris et al., 2019; Newman et al., 2011). It is also noteworthy that a lactate flux takes place from astrocytes to neurons, reinforced by the lactate gradient existing between these two cell types (González-Gutiérrez et al., 2020; Mächler et al., 2016; Zuend et al., 2020). As a consequence, some of the aforementioned activities, and in particular behavioral performances, may depend on such an intercellular flux, and thus on an efficient lactate transport on both astrocytes and neurons.

Lactate transport is mediated mainly by monocarboxylate transporters (MCTs) of the SLC16 solute carrier family (Bosshart et al., 2019; Halestrap, 2013). In the central nervous system three isoforms, MCT1, MCT2, and MCT4, have been described (Pierre et al., 2000; Pierre and Pellerin, 2005). MCT1 is highly expressed by endothelial cells but it is also found

on glial cells and some population of neurons. MCT2 is not only the main neuronal lactate transporter, but its expression has been reported also on some astrocytes, on oligodendrocyte precursor cells, newly formed oligodendrocytes, and microglia/macrophage cells. Initially, it was thought that MCT4 was exclusively expressed by astrocytes. However, new evidence suggest an important expression of this transporter on microglia/macrophage cells (Debernardi et al. 2003; Hanu et al., 2000; Pierre et al., 2000; Pierre and Pellerin, 2005; Zhang et al., 2014). Other studies also support the idea that the expression of each MCT in the central nervous system is not entirely cell-specific but more widespread and dynamically regulated (Kong et al., 2019; Moreira et al., 2009).

It was shown previously that the expression of both MCT1 and MCT4 increases in the hippocampal tissue of mice when exposed to the training session of the inhibitory avoidance (IA) paradigm (Tadi et al., 2015). This effect correlates with the increased extracellular lactate levels detected in the same brain region when performing an alternation task (Newman et al., 2011). A reduction in lactate transport produced either by knocking down MCTs using antisense oligonucleotides (Descalzi et al., 2019; Suzuki et al., 2011), via pharmacological inhibition (Korol et al., 2019; Newman et al., 2011) or using MCT haploinsufficient mice (Tadi et al., 2015) suggests that lactate shuttling between astrocytes and neurons is required for long-term memory formation. This conclusion was mainly based on data obtained in one-session training task (Y-maze alternation task, Newman et al., 2011; IA paradigm, Descalzi et al., 2019; Tadi et al., 2015; Suzuki et al., 2011). However, the importance of MCT activities for the formation of distinct types of memory remains unsettled, as well as their putative role in the learning process. Besides, the methodologies employed in previous studies may not be refined enough to unravel the separate contribution of specific cell types.

In order to better understand the involvement of lactate and its cell-specific transport in cognition, we used mouse models in which we selectively reduced the expression of either

neuronal MCT2 or astrocytic MCT4 in the dorsal hippocampus, a brain region critical for long-term episodic memory formation. To examine the contribution of each of those MCTs in hippocampus-dependent learning and memory, we employed a series of behavioral tasks. Results obtained show the differential participation of neuronal MCT2 and astrocytic MCT4 in learning and memory. They also reveal the importance of MCT2 in mature neurons to preserve the process of adult neurogenesis in the dentate gyrus (DG).

2. Results

2.1 Strategy to disrupt the expression of neuronal MCT2 or astrocytic MCT4 in the dorsal hippocampus

In order to get insight about the importance of cell-specific lactate transport for behavior, conditional knockout (CKO) mice on a C57BL/6J background were generated in collaboration with Cyagen (Santa Clara, CA) for either MCT2 (MCT2^{f/f}) or MCT4 (MCT4^{f/f}) (Fig.1). Introduction of loxP sites flanking either exons 4 and 5 (MCT2^{f/f}, Fig.1A) or exons 3, 4 and 5 (MCT4^{f/f}; Fig.1B) was obtained by homologous recombination. Generation of heterozygous or homozygous animals carrying the floxed allele was verified by PCR with appropriate sets of primers as shown for each genotype. Young adult male MCT2^{f/f} and MCT4^{f/f} mice with a minimum of 10 backcrossed generations were used for the main experiments of the present work.

Given that the contribution of the dorsal hippocampus to cognitive functions has been extensively described (Fanselow and Dong, 2010; Strange et al., 2014), we decided to target this specific brain region to induce the recombination and consequent reduction of MCTs expression. With the aim to discriminate the contribution of neuronal and astrocytic lactate transport, we induced cell-specific targeted recombination in this brain region via the stereotaxic injection of adeno associated virus-based vectors (AAV) (Fig. 2A, C). We employed

AAV-hSyn-GFP-cre for neurons or AAV-GFAP-GFP-cre for astrocytes, while corresponding control AAVs (AAV-hSyn-EGFP and AAV-GFAP-EGFP) were used in parallel. AAVs diffused and spread over the entire anteroposterior axis of the dorsal hippocampus, notably in the DG but also at least partially in other subregions, with a large tropism for the corresponding cells (Fig. 2B, D).

Three weeks after AAV injections, whole dorsal hippocampi were dissected and analyzed for gene as well as protein expression. Downregulation of Slc16a7 gene expression and of the corresponding MCT2 protein was confirmed in MCT2^{f/f} mice treated with the appropriate AAV-cre (Fig. 3A, C, E). Similarly, MCT4^{f/f} mice that received the AAV-cre injections exhibited decreased expression levels of the Slc16a3 gene and of the corresponding MCT4 protein (Fig. 3B, D, F). Interestingly, decreased expression of MCT2 caused an upregulation of MCT4 mRNA levels (Fig. 3A), while decreased expression of MCT4 induced upregulation of MCT1 protein expression (Fig. 3D, F). A possible impact on glucose transport or on excitatory neurotransmission was also evaluated by measuring mRNA expression levels of glucose transporters as well as of AMPA and NMDA receptor subunits. MCT2 and MCT4 reduced expression levels had no effect on mRNA expression of GLUT1 (Slc2a1) or GLUT3 (Slc2a3), as well as of GluA1 (Gria1), GluN1 (Grin1) and GluN2 (Grin2) subunits (Supplementary Fig. 1A, B). Interestingly, MCT2 (but not MCT4) reduced expression levels caused a selective reduction of the AMPA receptor GluA2 subunit at both the mRNA and protein levels (Supplementary Fig. 1C, D).

2.2. Overview of basic behavior in mice with hippocampal MCT2 or MCT4 reduced expression levels

Prior to determine the impact of disrupting neuronal or astrocytic lactate transport on behavior, performances of sham MCT2^{f/f} and MCT4^{f/f} mice were evaluated and compared with

those of similar background strain (C57BL/6J) mice. C57BL/6J mice injected i.p. with the noncompetitive antagonist of the N-Methyl-D-aspartate receptor, MK-801, were used as positive controls for altered behavior (van der Staay et al., 2011) in the cognitive tasks chosen (Supplementary Fig. 2). In the 90-min and 24-h version of the novel object recognition (NOR) task, strong recognition memory was exhibited by sham MCT2^{f/f} or MCT4^{f/f} mice and WT mice, as indicated by the significantly higher time spent exploring the novel object (recognition index above 0.5; Supplementary Fig. 2B). As expected, only MK-801-treated animals displayed a significant reduction of this parameter in the 24-h version of the test. In the Morris water maze (MWM) task, the learning curve showing the time to find the platform on each training day was comparable between the groups except for MK-801-treated mice (Supplementary Fig. 2C). We found no differences between all groups in the probe trial evaluating the time spent in the target quadrant (TQ). However, we noticed a slightly higher swimming speed for sham MCT2^{f/f} as compared with WT (Supplementary Fig. 2A).

Three weeks after stereotaxic surgery, mobility, anxiety, motivational behavior, and working memory of mice with reduced expression levels of neuronal MCT2 or astrocytic MCT4 were assessed and compared to MCT2^{f/f} and MCT4^{f/f} mice treated with the corresponding control viral vectors (Supplementary Fig. 3A). No effect on mobility and thigmotaxis was detected in the open field task (Supplementary Fig. 3B). To further probe anxiety, mice were tested in the elevated plus-maze and the odor predator test. Only mice with reduced expression levels of MCT4 spent a significantly longer time in the closed arms of the elevated plus-maze, compared to their corresponding control, although it was not strikingly different from the other groups (Supplementary Fig. 3C). In the odor predator test, the immobility time rose when mice were exposed to the major component of the anal gland secretions of the red fox 4,5-dihydro-2,4,5-trimethyl-thiazole (TMT), but there were no differences between ctrl and cre groups (Supplementary Fig. 3D). The forced swimming test

provided similar time scores in immobility, swimming, or climbing between the mice with decreased levels of MCT2 or MCT4 and their corresponding controls (Supplementary Fig. 3E). Results of the Y-maze test revealed no significant differences in the percentage of spontaneous alternation between the different treatments, although a small tendency for a decrease was visible in both MCT2^{f/f} and MCT4^{f/f} mice treated with AAV-cre injection (Supplementary Fig. 3F).

2.3. Analysis of memory after a brief (90-min) or longer (24-h) delay in mice with disrupted expression of hippocampal MCTs

Behavioral tasks that included a small training period (1-2 trials) followed by a short interval (≤ 24 h) before testing memory were used to further probe hippocampal function (Fig. 4A). In the IA task, a substantial decrease in the latency to enter the dark compartment where they previously (24 h before) received a mild electrical shock to the paws was observed for both MCT2^{f/f} and MCT4^{f/f} mice treated with the AAV-cre (Fig. 4B).

To examine whether lactate transport may be necessary for memory formation in a different context (not fear-related), recall after a brief (90 min) or longer (24 h) delay was investigated with the NOR task. With a 90-min interval between training and the probe session, the performance in mice with reduced expression levels of either the astrocytic MCT4 or the main neuronal lactate transporters showed a considerable increase in the exploring time of the novel object, reaching significant recognition indexes above the 0.5 chance level (Fig. 4C). When investigating recall after a 24-h delay, groups treated with the corresponding control AAV showed a clear preference for exploring the novel object. However, mice with reduced levels of either neuronal MCT2 or astrocytic MCT4 exhibited recognition indexes close or below chance level, meaning no preference for any object in the probe test (Fig. 4D).

2.4. Detailed analysis of spatial learning and 7-days memory

IA and NOR are tasks that require during acquisition, consolidation, and retrieval of the information a well-coordinated involvement of many brain areas and not just the hippocampus (Barker and Warburton, 2011; Izquierdo et al., 2016). In order to pursue a more refined analysis of the involvement of MCTs in learning processes involving this brain region, the MWM task was used, as it was also described to be more hippocampus-dependent (Vorhees and Williams, 2006). As indicated in Fig. 5A, the protocol included repeated trials across several days that allowed evaluating spatial learning as well as reference memory in the probe trial. The learning curve in the water maze revealed a significant delay in the time to find the platform (days 2 and 3) in mice with reduced expression levels of neuronal MCT2, as compared with their control group (Fig. 5C). A similar effect was also present but less extended (only day 2) in mice with diminished MCT4 (Fig. 5F). Interestingly, for both groups this alteration faded out as training trials continued (Fig. 5C and F, days 4-6).

An attempt to rescue behavioral performance in mice with decreased MCT levels was carried out by a constant i.c.v. infusion with lactate (30 $\mu\text{mol/day}$) exclusively during the training phase by employing osmotic minipumps (Fig. 5A). First, we confirmed by microdialysis in freely-moving mice a significant increase of extracellular lactate concentration within the dorsal hippocampus in those animals by about 2.5 fold (Fig. 5B). Concerning behavior, while for mice with reduced MCT2 levels performance persisted with higher time to find the platform compared with its control (Fig. 5C), lactate rescued learning proficiency in mice with decreased levels of MCT4 (Fig. 5F). As observed before, in the last three training days in the MWM, all groups achieved similar latency times as their controls. Finally, disrupting the expression in the of neuronal MCT2, but not of astrocytic MCT4, significantly decreased the time spent in the TQ in the probe trial. Lactate treatment did not modify this parameter for neither MCT2^{f/f} nor MCT4^{f/f} mice (Fig. 5D, E and G, H respectively).

2.5. Neurogenesis in mice with hippocampal MCT2 or MCT4 reduced expression levels

Since it has been demonstrated that disrupting neurogenesis causes spatial memory impairment (Jessberger et al., 2009; Martinez-Canabal et al., 2013), a possible impact of reduced MCT expression levels on this process was investigated in our mouse models. Thus, we analyzed the expression of canonical early (sex determining region Y- box 2, Sox2) and late (doublecortin, DCX) histological markers associated with adult-born dentate granule cells development in dorsal hippocampus (Couillard-Despres et al., 2005; Suh et al., 2007). Reduced expression levels of either neuronal MCT2 or astrocytic MCT4 did not modify the number of Sox2 positives (Sox2+) cells specifically located in the subgranular zone (SGZ) of the DG (Fig. 6A, B). Interestingly, mice with reduced neuronal MCT2 levels exhibited not only modified distribution but also altered morphology of DCX labeled cells (Fig. 6C). Quantitative analysis revealed a significant reduction in the size of the DCX positive area (Fig. 6D). In addition, these features in mice with reduced expression levels of neuronal MCT2 were accompanied by argyrophilic patterns detected by a silver staining of the dorsal hippocampus (Fig. 6E). In contrast, none of these changes were observed in MCT4^{f/f} mice.

3. Discussion

Previous observations have suggested a role of intercellular lactate exchange and metabolism in memory formation (Korol et al., 2019; Suzuki et al., 2011). However, to what extent lactate transporters in either neuronal or astrocytic cells are important in learning vs. memory, and by acting via similar mechanisms or not, had remained elusive. Here we provide evidence that lactate transport via MCTs in both hippocampal astrocytes and neurons facilitates learning of spatial tasks, while lactate transport in adult neurons is uniquely involved in the

maturation of newborn neurons in the DG, thus being essential for the formation of spatial memories.

Different approaches such as pharmacological inhibitors and anti-sense oligonucleotides have been used so far to study the involvement of lactate transport in memory (Korol et al., 2019; Suzuki et al., 2011). In this study, we described and used new CKO mouse strains for the monocarboxylate transporters MCT2 and MCT4. Our initial characterization of those mice (Supplementary Fig. 2) indicates that these CKO mouse strains are not entirely equivalent to the WT C57BL/J background strain, but nevertheless reliable to test behavioral performances. Taking advantage of these MCT2^{f/f} and MCT4^{f/f} animals, we wanted to determine if there was a different contribution of neuronal and astrocytic lactate transporters in learning and memory. For this, we induced cell-specific targeted recombination using AAVs. The hippocampus is a brain region well-studied in rodents for its involvement in several behavioral tasks. Particularly, the dorsal part has an important role in processing spatial information (Moser and Moser, 1998; Strange et al., 2014). Therefore, we chose to induce targeted recombination of either neuronal MCT2 or astrocytic MCT4 in this brain area via stereotaxic injection of the corresponding AAVs. Our results in Fig. 2 confirm the cell specificity of our experimental approach.

We managed to decrease significantly, although partially, gene expression and protein of neuronal MCT2 or astrocytic MCT4 in the targeted area, results expected from the analysis of the whole dorsal hippocampal tissue that indeed contains some cells not targeted by the corresponding AAVs. The disruption of MCT2 expression induced an increase in MCT1 mRNA, meanwhile the decreased MCT4 expression promoted an increase in MCT1 protein levels. Such responses could be a compensation attempt in response to a disturbed lactate supply within the targeted area. Modifications in MCT expression and reorganization have been previously reported when animals were exposed to energetically challenging conditions

(Rosafio et al., 2016; Rosafio and Pellerin, 2014), suggesting that MCTs represent an essential but adaptative system of energy supply. In contrast, no compensatory changes in expression were detected in either astrocytic or neuronal glucose transporters. We can not dismiss the possibility that glucose transport might be regulated by another mechanism such as the translocation of its transporters as described elsewhere (Fernandez et al., 2018; Simpson et al., 2008). However, based on the absence of a rescued phenotype when glucose is perfused i.c.v. (Supplementary Fig. 4), in contrast to lactate (Fig. 5F), it is unlikely that glucose and lactate are interchangeable substrates for some specific cognitive processes. Interestingly, the disruption of MCT2 expression led to a significant protein expression decrease of GluA2, an AMPA receptor subunit, supporting previous *in vitro* and *in vivo* data that suggested a common regulation mechanism between these two proteins (Maekawa et al., 2009; Pierre et al., 2009; Robinet and Pellerin, 2011).

The phenotype of mice can be strongly influenced by their genetic background and targeted genetic modifications (Lengacher et al. 2013; Matsuo et al., 2010). Notably, physical variations in perception and locomotion, as well as increased anxiety and motivational problems can disrupt mouse performance in a variety of behavioral tests. Therefore, we first analyzed those parameters in mice with reduced hippocampal levels of MCT2 or MCT4. The absence of changes in tasks such as the open field, the elevated plus-maze and the odor predator test, suggests no particular anxiety phenotype, especially under stressful conditions. In addition, the forced swimming test revealed no motivational differences between all groups. We also studied working memory in the Y-maze but no significant alteration (despite a tendency) in working memory could be evidenced using the spontaneous alternation task, a behavioral performance known to involve hippocampal activity (Conrad et al., 1996). This last result differs from those obtained by pharmacologically inhibiting MCT2 with α -cyano-4-hydroxycinnamate, which was found to significantly impair the alternation scores in the same test (Newman et al., 2011).

This difference may be due to 1) the limited extent of neuronal MCT2 reduced expression levels within the hippocampus in our mice; 2) the possible effects of α -cyano-4-hydroxycinnamate at high concentrations on other targets than MCTs and/or on different MCT isoforms simultaneously (Bröer et al., 1999; Dimmer et al., 2000; Halestrap and Denton, 1974). This point however will need further investigation to be resolved.

Our behavioral evaluation of recall after a 90-min delay in the NOR task did not reveal any difference between our cre-treated groups and their corresponding controls, indicating no alterations in neither the acquisition of information nor short-term (90-min) memory. Pharmacological inhibition or antisense knockdown of hippocampal MCTs led to similar results in related short-term memory tests (Korol et al., 2019; Suzuki et al., 2011). When evaluating the same task, but after an interval of 24 h between the training trial and the probe test, mice with reduced expression of MCT2 or MCT4 exhibited a substantial impairment in recognition of the novel object. These data are comparable to the altered recall after a 24-h delay evidenced in the IA task. Thus, our results are in agreement with a previous study using the same IA task but a different animal model and experimental interfering approach (i.e. antisense oligonucleotides in rat) supporting the idea that astrocyte-neuron lactate shuttling is essential for establishing long-term (24-h) memory (Suzuki et al., 2011). Our data from the NOR and IA tests suggest that hippocampal neuronal and astrocytic MCTs are required to form long-term (24-h) memory, but not acquisition or short-term (90-min) memory, in tasks at least partially dependent on the dorsal hippocampus. These results are consistent with the proposed role of lactate as an essential energy source to support the high-energy demand for *de novo* mRNA translation critical for long-term memory consolidation (Descalzi et al., 2019). Interestingly, alterations in glutamate neurotransmission cause similar effects on long-term (24-h) memory of mice, as shown in our group of mice treated with MK-801. Considering that mice with reduced expression levels of neuronal MCT2 also showed reduced levels of GluA2, further

investigation was needed to determine if the effects of reduced MCT2 expression levels could be due to a possible alteration of GluA2-mediated neurotransmission (see below).

The MWM test was used to refine our understanding of the involvement of MCTs in hippocampus-dependent learning and memory processes (Vorhees and Williams, 2006). The fact that mice with reduced expression levels of neuronal MCT2 or astrocytic MCT4 exhibited a delay in learning, but were able to reach the same latency time in the last training days, suggests at least an implication of hippocampal MCTs in the acquisition of spatial information. These data agree with previous evidence that lactate production at specific time periods of learning is essential (Gibbs et al., 2006; Harris et al., 2019). The selective non-competitive GluA2 subunit antagonist perampanel (PER) demonstrated a similar effect on the learning curve as mice with reduced MCT2 levels (Supplementary Fig. 5A). This observation confirmed the relevance of AMPA subunits integrity for spatial learning (Zhou et al., 2018). But it also suggests that the effect of reduced expression levels of neuronal MCT2 on spatial learning could be related (at least in part) to an altered expression of GluA2 subunit as revealed previously (Supplementary Fig. 1C). In contrast, the impact of reduced expression levels of astrocytic MCT4 on spatial learning could be rather explained by a lactate effect *per se*, as the level of performance is rescued by an intracerebral infusion of this molecule (Fig. 5F), but not by glucose (Supplementary Fig. 4C). Indeed, this recovery experiment with lactate infusion and the subsequent learning improvement in mice with disrupted expression of astrocytic MCT4 (but not neuronal MCT2) suggest that lactate supply by astrocytes (via MCT4) and its neuronal uptake (via MCT2) are essential to sustain learning efficiency.

The MWM probe test revealed some additionally meaningful information. Mice with reduced expression of astrocytic MCT4, after having learned the task, could recall such information after 7 days. It can not be excluded that the MCT1 upregulation detected on those mice may compensate the altered MCT4 expression on astrocytes and provide the necessary

energy and metabolic requirement for memory consolidation. However, *in vitro* data suggested that this transporter is mainly responsible for tonic lactate efflux from astrocytes (Maekawa et al., 2008), while MCT4 expression is regulated dynamically by various neuronal or exogenous stimuli to accommodate enhanced glycolytic rates (Brix et al., 2012; Marcillac et al., 2011; Rosafio and Pellerin, 2014). Apart from MCT1, lactate channels (Sotelo-Hitschfeld et al., 2015; Zuend et al., 2020), connexin/pannexin based-channels (Karagiannis et al., 2016; Rouach et al., 2008) or the aquaglyceroporin 9 (Badaut, 2010) could also contribute to facilitate the passage of lactate across membranes and compensate for the absence of MCT4 on astrocytes. On the contrary, although mice with reduced expression levels of neuronal MCT2 encoded the task data, they could not recall such information. In the MCT2^{f/f} mice, we could demonstrate that the effect was MCT2-dependent *per se* and not related to alteration in GluA2 expression since PER treatment did not induce deficits in very long-term (7-d) memory (Supplementary Fig. 5B). Moreover, based on the negative results from the recovery experiment with lactate in MCT2^{f/f} mice and the lack of effect in the probe trial, involvement of other lactate-driven mechanisms such as the activation of the HCAR1 (Lauritzen et al., 2014), which modulates neuronal activity (de Castro Abrantes et al., 2019) can be dismissed. Consequently, these findings imply that neuronal MCT2 and lactate uptake in the hippocampus, but not an intact astrocytic lactate flux via MCT4, is crucial for very long-term (7-d) memory formation.

It is known that exogenous lactate increases adult neurogenesis in mice (Lev-Vachnish et al., 2019), and that careful control of lactate concentration is determinant for this process (Wang et al., 2019). The disrupted expression of neuronal MCT2 or astrocytic MCT4 in the hippocampus did not disturb the number of Sox2⁺ adult neural stem progenitor cells, as demonstrated by the quantitative analysis of Sox2⁺ cells in the in the SGZ of the DG. Although it has been shown that neuronal progenitor maintenance requires lactate metabolism (Álvarez et al., 2016), our observation implies that monocarboxylates transport via MCTs in both adult

neurons and astrocytes is not essential for the first stages of adult hippocampal neurogenesis. In order to assess the generation of immature neurons derived from adult neurogenesis, we then examined DCX positive cells in the DG (Couillard-Despres et al., 2005). Strikingly, reduced expression levels of neuronal MCT2 (but neither astrocytic MCT4 reduced expression levels, nor a PER treatment, Supplementary Fig. 5C, D) altered the morphology, distribution and positive area for DCX, correlating with the impaired very long-term (7-d) memory observed in the MWM. In brain tissue of the same mice, we found more intense argyrophilic areas, an indication of degeneration. Adult neurogenesis is considered a mechanism of hippocampal plasticity. A decrement or alteration in this process has been linked to cognitive impairment (Berdugo-Vega et al., 2020; Jessberger et al., 2009; Martinez-Canabal et al., 2013), what could explain the behavioral data of our MCT2^{f/f} mice. Considering that neuronal MCT2 expression was reduced in adult neurons, our results suggest that lactate transport in adult neurons of the hippocampus is key for neuronal maturation during hippocampal neurogenesis. It also implies an indirect, non-cell autonomous effect of lactate. Those results would be consistent with the description that lactate flux in brain is key to maintain neuronal activity (González-Gutiérrez et al., 2020), which would provide essential neuronal activity-dependent signal(s) contributing to the neurogenic niche to promote neurogenesis (Parent et al., 1997; Stone et al., 2011). However, the identity of such signal(s) remains to be determined. Our data also imply that MCT4 in astrocytes does not seem essential for adult hippocampal neurogenesis, although a participation of the aforementioned compensatory mechanisms for the transport of monocarboxylates in those cells can not be excluded.

In conclusion, our results highlight the differential participation of neuronal and astrocytic lactate transporters to hippocampal-dependent learning and memory processes. We also provide further evidence of the importance of lactate use in adult neurons to promote normal neurogenesis in the hippocampus. These results emphasize the role of lactate transport

in cognition and associated processes that goes beyond its simple role in alternative energy substrate supply or waste disposal.

4. Methods

4.1. Animals

We used adult male mice of different strains. Conditional knockout (CKO) mice for MCT2 are referred in the text as MCT2^{f/f}, while CKO for MCT4 are named MCT4^{f/f}. CKO background strain was C57BL/6J. These mice were considered as WT. Mice were group-housed (3-5/cage) while cardboard cylinders and tissue were provided as cage basic enrichment and nest material. Mice were housed in a laboratory environment with controlled temperature and 12 h light/dark cycle, with food and water *ad libitum*. All experiments were carried out at the Department of Physiology of the University of Lausanne, Switzerland. All procedures aimed to fulfill the criteria of the 3Rs and were approved by the Veterinary Offices of Vaud (Switzerland, license number 3229.a).

4.2. Surgical procedures

Surgery. In all surgical procedures, mice were anesthetized by inhalation of a mixture of oxygen and isoflurane (5% for the induction and 2-1% during surgery). In addition, an analgesic (buprenorphine) was administered s.c. at a dose of 0.1 mg/kg before the incision. During surgery, mice were placed over a heating pad to maintain their body temperature. At the end of this surgical intervention, we supplied paracetamol in the water (500 mg/cage) during three days.

Viral vector injection. Mice were 8 weeks old when viral vector injection was performed. Mice were bilaterally injected into the dorsal hippocampus (AP -2.3 mm, L \pm 1.90 mm, DV -1.3 mm), one of the four different AAVs (Vector Core, University of North Carolina). Injections of 1.0 μ l (4.7×10^9 particles/ μ l) per site for AAV8-hSyn-GFP-cre and AAV8-hSyn-

EGFP were made, while for AAV8-GFAP-GFP-cre and AAV8-GFAP-EGFP, injections of 1.5 μl (4.10×10^9 particles/ μl) were done. Viral vector injected volumes were chosen based on preliminary results to cause a reduced expression of the protein of interest. Skin was sutured using 4.0 sterile suture thread.

i.c.v. lactate or glucose infusion. This surgical procedure was performed six days before the first handling session on animals that underwent behavioral evaluations. It ensured the infusion of the corresponding molecule during the training sessions of the MWM task. Sodium L-lactate (L7022, Sigma-Aldrich) or D-glucose (A3666, Panreac Applichem) were dissolved in sterile isotonic saline solution (vehicle, veh), pH = 7.4. Osmotic minipumps (Alzet model 1002, flow rate 6 $\mu\text{l}/\text{day}$) were filled with veh or the substrate solution to infuse 30 $\mu\text{mol}/\text{day}$ of lactate or 15 $\mu\text{mol}/\text{day}$ of glucose. Then, they were incubated in sterile isotonic saline solution at 37° for 12 h for stabilization before the implantation. The day of surgery, mice were anesthetized as described above. Brain infusion cannula (brain infusion kit 3, Alzet) were implanted to target the lateral ventricle (AP -0.6 mm, L -1.5 mm, DV -2.1 mm). Cannula were glued to the skull using a small drop of cyanoacrylate adhesive, and the other cannula end was connected to the osmotic pump that was placed subcutaneously in the back of the animals. Finally, the cannula implant was covered and fixed with dental cement.

i.c.v. PER infusion. This experiment was performed in MCT2^{ff} mice. Surgery of implantation was carried out six days before the first handling session for the MWM test. It ensured PER infusion during the training sessions and the probe test of the MWM task. Perampanel (A12498, Adooq Biosciences) was dissolved in DMSO and a suspension (5% v/v final DMSO concentration) in saline solution (veh), pH = 7.4 was prepared. Osmotic minipumps (Alzet model 1004, flow rate 2.64 $\mu\text{l}/\text{day}$) were filled with veh or PER suspension to infuse 0.043 $\mu\text{mol}/\text{day}$. Other PER doses were tested but the highest one that did not induced

a sedative effect was selected. The rest of the process to i.c.v. implant the minipumps was completed as described above.

4.3. Microdialysis

Sham MCT2^{f/f} mice were 9 weeks old when surgery was performed. This cohort of mice was not exposed to behavioral evaluations. The day of surgery, mice were anesthetized as described above. A screw was placed into the frontal bone of the skull to serve as an anchor. The cannula guide (CMAP000137-CMA 7 cannula guide, Harvard Apparatus) was implanted to target the dorsal hippocampus (AP -2.3 mm, L +1.90 mm, DV -1.3 mm), and fixed with dental cement. Seven days after the cannula guide implantation (mimicking the normal time for WM training), microdialysis was carried out in awake, freely moving mice. Previously, water-flushed microdialysis probes (CMAP000082-CMA 7 probe, Harvard Apparatus) were inserted into the cannula guide. Animals were then placed in the bowl of a free-movement microdialysis system, and cannulas were continuously perfused using CMA perfusion fluid (CMAP000034, Harvard Apparatus) at a flow rate of 2 μ l/min. After a 2 h equilibration period, the perfusate was collected, immersed in liquid nitrogen and stored at -80 °C for later analysis. Lactate concentration was determined using the colorimetric assay of the L-Lactate Assay Kit (ab65330, Abcam), following the instructions of the manufacturer.

4.4. Behavioral evaluations

Behavioral evaluations were carried out three weeks after AAV injections. In animals without surgery, the evaluation was made at paired age (11 weeks old). Each behavioral test was performed in independent groups. Two days of handling with the experimenter and habituation in the experimental room were included before each behavioral test. In addition, before everyday session, mice were allowed to acclimatize to the experimental room for 1 h

prior to start the test. All behavioral evaluations were video recorded and analyzed with ANY-Maze software. When applicable, to avoid odor traces, the arena (and objects) was cleaned with 10% ethanol followed by water, and dried with paper towel between trials. For all animals included in the study, the correct injection of the corresponding AAV was confirmed by detecting the reporter protein in hippocampus of dissected brains. When indicated, MK-801 (0.1 mg/kg) in sterile isotonic saline solution was i.p.-administered 30 min before the beginning of the test. In the following tasks, visual interferences were prevented by using curtains around the diverse arenas.

Speed. Walking speed was evaluated during a 5 min session in an open field arena, while swimming speed was determined during a 90 s session with a visible platform in the water maze.

Open-field. The open-field arena consisted of an enclosed square-shaped area (50 cm/side). Mouse was placed in the center of the arena, and allowed to freely explore during 1 trial, 15 min.

Elevated plus-maze. Mouse was placed at the intersection of the open and closed arms, and allowed to freely explore during 1 trial, 5 min.

Predator odor test. During three days (1 trial, 10 min/each day), the mouse was placed in the arena (70 x 30 cm) having on one side a petri dish containing cotton with 50 μ l of a solution 1:1 of ethanol and water (veh). The day of the experiment, 1 trial (10 min) was performed. In this case, before placing the mouse, 50 μ l of a solution 5 % of TMT (CTK1C8970, ChemTik) diluted in veh was added in the petri dish. This protocol was based on a previous study (Nasca et al., 2013) and standardized for our laboratory conditions.

Forced swimming test. A transparent cylindrical tank (30 cm height x 20 cm diameter) was filled with water at ~ 24 °C, to a level such that the animal was not able to touch the floor or escape. The mouse was placed in the water for 1 trial (4 min), and its behavior was videotaped

using a lateral view of the tank. At the end of each session, the mouse was allowed to dry using a cage full of tissue placed under a heating lamp. This procedure and the video analysis was based on a previous study (Can et al., 2012).

IA. The IA chamber consisted of a rectangular-shaped box divided into a safe compartment (painted white and illuminated), and a shock compartment (painted black and dark). A sliding door separated those compartments and the grid floor allowed us to deliver a slight foot shock when necessary. The IA task required one training session and one probe trial separated by an interval of 24 h. During the training session, the mouse was placed in the safe compartment facing away from the door. After 10 sec, the door was opened, giving the animal access to the shock chamber. When the entire body of the mouse was in the dark chamber, the door was closed, and after a 5 s delay, a brief foot shock (0.3 mA, 2 s) was delivered to the mouse. After 5 s, the door was opened and the animal could return to the safe compartment. In the probe trial, this procedure was repeated, but no foot shock was delivered. A maximum time of 5 min was given to the mouse to enter the shock compartment. This protocol was based on another one used for rats (Garín-Aguilar et al., 2014), but the intensity of the electroshock was adapted as moderate for mice (Canto-de-Souza and Mattioli, 2016).

NOR. This task required three stages. One day for habituation in an empty arena (2 trials, 10 min/each), followed by training (2 trials, 10 min/each), separated by an interval of 90 min or 24 h from the probe session (1 trial, 3min). Test was performed in the open-field arena. For the training session, two identical objects (50 ml falcon tubes containing white water, familiar objects) were placed equidistant from the center and walls of the arena. For the probe session, one object was replaced with a new one that was visually distinct from the others (50 ml plastic bottle flat-shape containing white water, novel object). The efficacy of the chosen object to be discriminated in this task was verified in preliminary experiments. The location of the novel object was counter-balanced among animals. In each trial, the mouse was allowed to explore

the objects freely. Exploration was considered effective when the nose of the mouse was ~1 cm or closer to the object and facing it. Climbing was not considered exploration. Mice were discarded from the experiment if they did not reach ≥ 10 s of total time of exploration in the probe session. The index of preference was calculated as (time exploring the object of interest) divided by (total time of exploration considering both objects). An index value over 0.5 was considered as a preference.

Cues located on the walls of the room were included for the following tasks:

Y-maze. Mouse was placed at the end of one arm, and allowed to freely explore for 1 trial, 5 min. Spontaneous alternation was considered valid when the animal visited all three arms without going into the same arm twice in a row. The alternation score was calculated considering the first 2 min of the trial. The percentage of spontaneous alternation was determined by dividing the number of alternations by the number of total visits x 100.

MWM. This protocol is based in others previously reported (Morris, 2015; Vorhees and Williams, 2006). A circular maze (40 cm height x 150 cm diameter, black) was used. The maze was filled with water and its temperature maintained across trials close to 24 °C. White tempera paint was used to color water. MWM protocol included 6 training days (4 trials/day and only 2 trials in the last one), a resting interval of 7 days, and the probe test (1 trial, 40 s). A transparent circular-shaped platform (12 cm) located in the center of a specific quadrant of the maze and hidden by the white water was used during training. In each training trial, the animal was introduced into the pool at one of the four starting points. The mouse was allowed to swim for a maximum of 60 s or until it located the platform. If the animals did not find the platform within the time limit, it was led to it and then, it was allowed to stand on the platform for 20 s. In the probe trial, the platform was removed. At the end of each trial, the mouse was dried using a cage full of tissue placed under a heating lamp. Heatmap images include the cumulative body

trajectory/group, and were obtained with ANY-Maze software from the information of the probe trial.

4.5. Molecular biology techniques

Tissue dissection. For mRNA and protein analyses, mice were euthanized by cervical dislocation followed by decapitation. Brain was dissected on an ice-cold plate. A mouse brain matrix was used to obtain coronal slices. The presence of the reporter protein was confirmed by epifluorescence microscopy followed by isolation of the dorsal hippocampus. The tissue was immediately frozen in liquid nitrogen and stored at -80 °C for later analyzes.

RT-qPCR. RNA extractions were performed with the RNeasy Mini Kit (74106, Qiagen). All extractions were performed on ice under RNase free conditions, with ultrapure sterile RNase-DNase free water. RNA pellet was finally suspended in 40 µl of ultrapure water and stored at -80 °C. RNA concentration was determined, and samples with aberrant A260/280 or A260/230 ratios were discarded. Mouse mRNAs were reverse transcribed using SuperScript™ II Reverse Transcriptase kit (18064014, Invitrogen, Thermo Fisher Scientific). cDNAs were amplified by PCR with Power SYBR™ Green PCR Master Mix (4367659, Applied Biosystems, Thermo Fisher Scientific). For this last step, a concentration of 150 nM was used for the cDNA of housekeeping genes and 300 nM for the rest. Primers were used at a concentration of 10 µM/each. Primers used in this study are listed in Supplementary Table 3.

Western blot. Proteins were extracted with RIPA lysis buffer (20-188, Millipore) completed with protease and phosphatase inhibitors (78444, Thermo Fisher Scientific). Protein concentration was determined using Micro BCATM Protein assay kit (23235, Thermo Fisher Scientific). Proteins were separated with a homemade 10 % SDS-PAGE gel using 20 µg protein/well. A semi-dry TransBlot-Turbo™ transfer system (BIO-RAD) was used to transfer proteins to nitrocellulose membranes. Transfer efficiency was confirmed by staining with

homemade Ponceau S solution. Membranes were washed with 0.1 % Triton X-100 in phosphate-buffered saline solution (this product was also used for the following washing procedures). Then, the membrane was blocked for 1 h with Odyssey Blocking Buffer (927-40000, LI-COR Biosciences). Antibodies were prepared in the same blocking buffer at the concentrations indicated in Supplementary Table 4. Membranes were incubated with continuous agitation with the primary antibody (overnight at 4 °C). They were washed followed by incubation with the secondary antibody (2h at room temperature). Membranes were revealed using the near-infrared fluorescence imaging system of LI-COR Odyssey, and images analyzed with the western blot analysis software Image Studio Lite (both systems from LI-COR Biosciences).

4.6. Histology

Mice for histological analysis were deeply anesthetized with pentobarbital and perfused transcardially with 50 ml saline solution (0.9 %), followed by 50 ml of 4 % paraformaldehyde in 0.1 M phosphate buffer, pH 7.4. Brains were removed, postfixed for 24 h at 4 °C, and transferred successively to 10, 20 and 30 % sucrose (24 h each). Immunohistochemistry was performed as previously described (Netzahualcoyotzi and Tapia, 2018), on freely floating fixed tissue sections. Antibodies used are listed in Supplementary Table 4. Imaging was done using a confocal microscope Zeiss LSM 780 GaAsP.

AAV diffusion and specificity. Thickness of brain sections was 30 µm. Pictures shown in Fig. 2 are a maximum intensity Z-projection (15 slices, 1 µm interval) obtained with ImageJ/Fiji.

Animals used for the following histological analyses completed the MWM protocol, except sham mice.

Sox2 quantification. Brain section thickness was 40 μm . Quantitative analysis was carried out manually using maximum intensity Z-projections of Sox2 pictures (12 slices, 2 μm interval) obtained with ImageJ/Fiji. Sox2+ cells specifically located in the SGZ were quantified. Three histological sections/mouse were analyzed and data average was reported as one data point in the graph. Pictures shown in Fig. 6A are 3-D representations obtained with Zen black 2012.

DCX quantification. Thickness of brain sections was 40 μm . This analysis was made with ImageJ/Fiji using maximum intensity Z-projections of DCX pictures of the whole dorsal hippocampus (5 slices, 1.08 μm interval). Using the thresholds tool, image was adjusted and measurement was limited by selecting only DG as the area of interest. The value obtained was normalized by the selected total area. Three histological sections/mouse were analyzed; then data were averaged, and reported as one data point in the graph. Pictures shown in Fig. 6C are a 3-D representations obtained with Zen black 2012.

Silver staining. Brain sections thickness was 30 μm . This staining was made using the FD NeuroSilver™ Kit II (FD NeuroTechnologies) following the instructions of the manufacturer. One μl injection into the dorsal hippocampus of 0.01 mM of 2-Amino-3-(3-hydroxy-5-methyl-isoxazol-4-yl) propanoic acid (AMPA) was used as a positive control tissue for neurodegeneration. Mice treated with AMPA were euthanized 24h after the injection. Pictures of silver staining shown in Fig. 6E and Supplementary Fig. 5C were obtained with bright-field microscopy.

4.7. Graphical representation.

All graphs and statistical analyses were performed using GraphPad Prism Software.

Author contributions

Conceptualization, C.N. and L.P. Performed the experiments, collected and analyzed the data, C.N. Wrote the original draft, C.N. Review & Editing C.N. and L.P. Funding Acquisition and Resources, L.P. Project Supervision, L.P.

Competing interests

The authors declare no competing interests.

Acknowledgements

We thanks Cendrine Repond for her support for molecular biology techniques and Marlen Knobloch for her suggestions for this work. L.P. received financial support for this project from the Department of Physiology, University of Lausanne and from the program IdEx Bordeaux ANR-10-IDEX-03-02.

References

- Álvarez, Z., Hyroššová, P., Perales, J.C., Alcántara, S., 2016. Neuronal progenitor maintenance requires lactate metabolism and PEPCCK-M-directed cataplerosis. *Cereb. Cortex.* 26, 1046-58. [https://doi: 10.1093/cercor/bhu281](https://doi.org/10.1093/cercor/bhu281).
- Badaut, J., 2010. Aquaglyceroporin 9 in brain pathologies. *Neuroscience.* 168(4):1047-57. [https://doi:10.1016/j.neuroscience.2009.10.030](https://doi.org/10.1016/j.neuroscience.2009.10.030).
- Barker, G.R., Warburton, E.C., 2011. When is the hippocampus involved in recognition memory? *J. Neurosci.* 31, 10721-31. <https://doi.org/10.1523/JNEUROSCI.6413-10.2011>.
- Berdugo-Vega, G., Arias-Gil, G., López-Fernández, A., Artegiani, B., Wasielewska, J. M., Lee, C. C., Lippert, M. T., Kempermann, G., Takagaki, K., Calegari, F., 2020. Increasing neurogenesis refines hippocampal activity rejuvenating navigational learning strategies

- and contextual memory throughout life. *Nat. Commun.* 11(1), 135.
<https://doi.org/10.1038/s41467-019-14026-z>.
- Bosshart, P.D., Kalbermatter, D., Bonetti, S., Fotiadis, D., 2019. Mechanistic basis of L-lactate transport in the SLC16 solute carrier family. *Nat. Commun.* 10, 2649.
<https://doi:10.1038/s41467-019-10566-6>.
- Bouzier-Sore, A.K., Voisin, P., Bouchaud, V., Bezancon, E., Franconi, J.-F. Pellerin, L., 2006. Competition between glucose and lactate as oxidative energy substrates in both neurons and astrocytes: a comparative NMR study. *Eur. J. Neurosci.* 24, 1687-1694.
<https://doi10.1111/j.1460-9568.2006.05056.x>.
- Brix, B., Mesters, J.R., Pellerin, L., Jöhren, O., 2012. Endothelial cell-derived nitric oxide enhances aerobic glycolysis in astrocytes via HIF-1 α -mediated target gene activation. *J. Neurosci.* 32(28):9727-9735. <https://doi:10.1523/JNEUROSCI.0879-12.2012>.
- Bröer, S., Bröer, A., Schneider, H. P., Stegen, C., Halestrap, A. P., Deitmer, J. W., 1999. Characterization of the high- affinity monocarboxylate transporter MCT2 in *Xenopus laevis* oocytes. *Biochem. J.* 341, 529-535. <https://doi.org/10.1042/0264-6021:3410529>.
- Brooks, G.A., 2018. The science and translation of lactate shuttle theory. *Cell Metab.* 27, 757-785. <https://doi:10.1016/j.cmet.2018.03.008>.
- Can, A., Dao, D.T., Arad, M., Terrillion, C.E., Piantadosi, S.C., Gould, T.D., 2012. The mouse forced swim test. *J. Vis. Exp.* 59, 3638. <https://doi:10.3791/3638>.
- Canto-de-Souza, L., Mattioli, R., 2016. The consolidation of inhibitory avoidance memory in mice depends on the intensity of the aversive stimulus: The involvement of the amygdala, dorsal hippocampus and medial prefrontal cortex. *Neurobiol. Learn. Mem.* 130, 44-51.
<https://doi:10.1016/j.nlm.2016.01.012>.
- Castillo, X., Rosafio, K., Wyss, M.T., Drandarov, K., Buck, A., Pellerin, L., Weber, B., Hirt, L., 2015. A probable dual mode of action for both L- and D-lactate neuroprotection in

- cerebral ischemia. *J. Cereb. Blood Flow Metab.* 35, 1561-1569.
<https://doi.org/10.1038/jcbfm.2015.115>.
- Conrad, C.D., Galea, L.A., Kuroda, Y., McEwen, B.S., 1996. Chronic stress impairs rat spatial memory on the Y maze, and this effect is blocked by tianeptine pretreatment. *Behav. Neurosci.* 110, 1321-34. <https://doi.org/10.1037/0735-7044.110.6.1321>.
- Couillard-Despres, S., Winner, B., Schaubeck, S., Aigner, R., Vroemen, M., Weidner, N., Bogdahn, U., Winkler, J., Kuhn, H.G., Aigner, L., 2005. Doublecortin expression levels in adult brain reflect neurogenesis. *Eur. J. Neurosci.* 21, 1-14. <https://doi.org/10.1111/j.1460-9568.2004.03813.x>.
- de Castro Abrantes, H., Briquet, M., Schmuziger, C., Restivo, L., Puyal, J., Rosenberg, N., Rocher, A.B., Offermanns, S., Chatton, J.Y., 2019. The lactate receptor HCAR1 modulates neuronal network activity through the activation of G α and G $\beta\gamma$ subunits. *J. Neurosci.* 39, 4422-4433. <https://doi.org/10.1523/JNEUROSCI.2092-18.2019>.
- Debernardi, R., Pierre, K., Lengacher, S., Magistretti, P.J., Pellerin, L., 2003. Cell-specific expression pattern of monocarboxylate transporters in astrocytes and neurons observed in different mouse brain cortical cell cultures. *J. Neurosci. Res.* 73, 141-55. <https://doi.org/10.1002/jnr.10660>.
- Descalzi, G., Gao, V., Steinman, M.Q., Suzuki, A., Alberini, C.M., 2019. Lactate from astrocytes fuels learning-induced mRNA translation in excitatory and inhibitory neurons. *Commun. Biol.* 2, 247. <https://doi.org/10.1038/s42003-019-0495-2>.
- Dimmer, K.S., Friedrich, B., Lang, F., Deitmer, J.W., Broer, S., 2000. The low-affinity monocarboxylate transporter MCT4 is adapted to the export of lactate in highly glycolytic cells. *Biochem. J.* 350, 219-227. <https://doi.org/10.1042/bj3500219>.
- El Hayek, L., Khalifeh, M., Zibara, V., Abi Assaad, R., Emmanuel, N., Karnib, N., El-Ghandour, R., Nasrallah, P., Bilen, M., Ibrahim, P., Younes, J., Abou Haidar, E., Barmo,

- N., Jabre, V., Stephan, J.S., Sleiman, S.F., 2019. Lactate mediates the effects of exercise on learning and memory through SIRT1-dependent activation of hippocampal brain-derived neurotrophic factor (BDNF). *J. Neurosci.* 39, 2369-2382. <https://doi:10.1523/JNEUROSCI.1661-18.2019>.
- Fanselow M.S., Dong, H., 2010. Are The Dorsal and Ventral Hippocampus functionally distinct structures? *Neuron.* 65, 7. <https://doi:10.1016/j.neuron.2009.11.031>
- Fernandez, A.M., Hernandez, E., Guerrero-Gomez, D., Miranda-Vizuet, A., Torres Aleman, I., 2018. A network of insulin peptides regulate glucose uptake by astrocytes: Potential new druggable targets for brain hypometabolism. *Neuropharmacology.* 136(Pt B):216-222. <https://doi:10.1016/j.neuropharm.2017.08.034>.
- Garín-Aguilar, M.E., Medina, A.C., Quirarte, G.L., McGaugh, J.L., Prado-Alcalá, R.A., 2014. Intense aversive training protects memory from the amnesic effects of hippocampal inactivation. *Hippocampus.* 24, :102-12. <https://doi:10.1002/hipo.22210>.
- Gibbs, M.E., Anderson, D.G., Hertz, L., 2006. Inhibition of glycogenolysis in astrocytes interrupts memory consolidation in young chickens. *Glia.* 54, 214-22. <https://doi.org/10.1002/glia.20377>.
- González-Gutiérrez, A., Ibacache, A., Esparza, A., Barros, L.F., Sierralta, J., 2020. Neuronal lactate levels depend on glia-derived lactate during high brain activity in drosophila. *Glia.* 68, 1213-1227. <https://doi:10.1002/glia.23772>.
- Halestrap, A.P., 2013. The SLC16 gene family - structure, role and regulation in health and disease. *Mol. Aspects Med.* 34, 337-49. <https://doi:10.1016/j.mam.2012.05.003>.
- Halestrap, A.P., Denton, R.M., 1974. Specific inhibition of pyruvate transport in rat liver mitochondria and human erythrocytes by alpha-cyano-4-hydroxycinnamate. *Biochem. J.* 1974;138:313–316. <https://doi:10.1042/bj1380313>.

- Hanu, R., McKenna, M., O'Neill, A., Resneck, W.G., Bloch, R.J., 2000. Monocarboxylic acid transporters, MCT1 and MCT2, in cortical astrocytes in vitro and in vivo. *Am. J. Physiol. Cell Physiol.* 278, C921-30. <https://doi.org/10.1152/ajpcell.2000.278.5.C921>.
- Harris, R.A., Lone, A., Lim, H., Martinez, F., Frame, A.K., Scholl, T.J., Cumming, R.C., 2019. Aerobic glycolysis is required for spatial memory acquisition but not memory retrieval in mice. *eNeuro.* 6, pii: ENEURO.0389-18.2019. <https://doi:10.1523/ENEURO.0389-18.2019>.
- Izquierdo, I., Furini, C.R., Myskiw, J.C., 2016. Fear memory. *Physiol. Rev.* 96, 695-750. <https://doi:10.1152/physrev.00018.2015>.
- Jessberger, S., Clark, R.E., Broadbent, N.J., Clemenson, G.D. Jr., Consiglio, A., Lie, D.C., Squire, L.R., Gage, F.H., 2009. Dentate gyrus-specific knockdown of adult neurogenesis impairs spatial and object recognition memory in adult rats. *Learn. Mem.* 16, 147-54. <https://doi:10.1101/lm.1172609>.
- Karagiannis, A., Sylantsev, S., Hadjihambi, A., Hosford, P.S., Kasparov, S., Gourine, A.V., 2016. Hemichannel-mediated release of lactate. *J. Cereb. Blood Flow Metab.* 36(7):1202-1211. <https://doi:10.1177/0271678X15611912>.
- Kong, L., Wang, Z., Liang, X., Wang Y, Gao L, Ma C., 2019. Monocarboxylate transporter 1 promotes classical microglial activation and pro-inflammatory effect via 6-phosphofructo-2-kinase/fructose-2, 6-biphosphatase 3. *J. Neuroinflammation.* 16, 240. <https://doi.org/10.1186/s12974-019-1648-4>.
- Korol, D.L., Gardner, R.S., Tunur, T., Gold, P.E., 2019. Involvement of lactate transport in two object recognition tasks that require either the hippocampus or striatum. *Behav. Neurosci.* 133, 176-187. <https://doi:10.1037/bne0000304>.
- Lauritzen, K.H., Morland, C., Puchades, M., Holm-Hansen, S., Hagelin, E.M., Lauritzen, F., Attramadal, H., Storm-Mathisen, J., Gjedde, A., Bergersen, L.H., 2014. Lactate receptor

- sites link neurotransmission, neurovascular coupling, and brain energy metabolism. *Cereb. Cortex.* 24, 2784-95. <https://doi:10.1093/cercor/bht136>.
- Lengacher, S., Nehiri-Sitayeb, T., Steiner, N., Carneiro, L., Favrod, C., Preitner, F., Thorens, B., Stehle, J.C., Dix, L., Pralong, F., Magistretti, P.J., Pellerin, L., 2013. Resistance to diet-induced obesity and associated metabolic perturbations in haploinsufficient monocarboxylate transporter 1 mice. *PLoS One.* 8, e82505. <https://doi:10.1371/journal.pone.0082505>.
- Lev-Vachnisch, Y., Cadury, S., Rotter-Maskowitz, A., Feldman, N., Roichman, A., Illouz, T., Varvak, A., Nicola, R., Madar, R., Okun, E., 2019. L-Lactate promotes adult hippocampal neurogenesis. *Front. Neurosci.* 13, 403. <https://doi:10.3389/fnins.2019.00403>.
- Mächler, P., Wyss, M.T., Elsayed, M., Stobart, J., Gutierrez, R., von Faber-Castell, A., Kaelin, V., Zuend, M., San Martín, A., Romero-Gómez, I., Baeza-Lehnert, F., Lengacher, S., Schneider, B.L., Aebischer, P., Magistretti, P.J., Barros, L.F., Weber, B., 2016. In vivo evidence for a lactate gradient from astrocytes to neurons. *Cell Metab.* 23, 94-102. <https://doi:10.1016/j.cmet.2015.10.010>.
- Maekawa, F., Minehira, K., Kadomatsu, K., Pellerin, L., 2008. Basal and stimulated lactate fluxes in primary cultures of astrocytes are differentially controlled by distinct proteins. *J. Neurochem.* 107(3):789-798. <https://doi:10.1111/j.1471-4159.2008.05650.x>.
- Maekawa, F., Tsuboi, T., Fukuda, M., Pellerin, L., 2009. Regulation of the intracellular distribution, cell surface expression, and protein levels of AMPA receptor GluR2 subunits by the monocarboxylate transporter MCT2 in neuronal cells. *J. Neurochem.* 109, 1767-78. <https://doi:10.1111/j.1471-4159.2009.06100.x>.
- Magistretti, P.J., Allaman, I., 2018. Lactate in the brain: from metabolic end-product to signalling molecule. *Nat. Rev. Neurosci.* 19, 235-249. <https://doi:10.1038/nrn.2018.19>.

- Marcillac, F., Brix, B., Repond, C., Jöhren, O., Pellerin, L., 2011. Nitric oxide induces the expression of the monocarboxylate transporter MCT4 in cultured astrocytes by a cGMP-independent transcriptional activation. *Glia*. 59(12):1987-1995. <https://doi:10.1002/glia.21240>.
- Margineanu, M.B., Mahmood, H., Fiumelli, H., Magistretti, P.J., 2018. L-lactate regulates the expression of synaptic plasticity and neuroprotection genes in cortical neurons: A transcriptome analysis. *Front. Mol. Neurosci.* 11, 375. <https://doi:10.3389/fnmol.2018.00375>.
- Martinez-Canabal, A., Akers, K.G., Josselyn, S.A., Frankland, P.W., 2013. Age-dependent effects of hippocampal neurogenesis suppression on spatial learning. *Hippocampus*. 23, 66-74. <https://doi:10.1002/hipo.22054>.
- Matsuo, N., Takao, K., Nakanishi, K., Yamasaki, N., Tanda, K., Miyakawa, T., 2010. Behavioral profiles of three C57BL/6 substrains. *Front. Behav. Neurosci.* 4, 29. <https://doi:10.3389/fnbeh.2010.00029>.
- Moreira, T.J., Pierre, K., Maekawa, F., Repond, C., Cebere, A., Liljequist, S., Pellerin, L., 2009. Enhanced cerebral expression of MCT1 and MCT2 in a rat ischemia model occurs in activated microglial cells. *J. Cereb. Blood Flow Metab.* 29, 1273-83. <https://doi:10.1038/jcbfm.2009.50>.
- Morland, C., Andersson, K.A., Haugen, Ø.P., Hadzic, A., Kleppa, L., Gille, A., Rinholm, J.E., Palibrk, V., Diget, E.H., Kennedy, L.H., Stølen, T., Hennestad, E., Moldestad, O., Cai, Y., Puchades, M., Offermanns, S., Vervaeke, K., Bjørås, M., Wisløff, U., Storm-Mathisen, J., Bergersen, L.H., 2017. Exercise induces cerebral VEGF and angiogenesis via the lactate receptor HCAR1. *Nat. Commun.* 8, 15557. <https://doi:10.1038/ncomms15557>.

- Morris, R.G.M., 2015. The Watermaze, in: Heather A. Bimonte-Nelson (Ed.), The maze book. Theories, practice, and protocols for testing rodent cognition. New York, pp. 73-92. <https://doi:10.1007/978-1-4939-2159-1>.
- Moser, M.B., Moser, E.I., 1998. Distributed encoding and retrieval of spatial memory in the hippocampus. *J. Neurosci.* 18, 7535-42. <https://doi.10.1523/JNEUROSCI.18-18-07535.1998>.
- Nasca, C., Orlando, R., Marchiafava, M., Boldrini, P., Battaglia, G., Scaccianoce, S., Matrisciano, F., Pittaluga, A., Nicoletti, F., 2013. Exposure to predator odor and resulting anxiety enhances the expression of the $\alpha 2 \delta$ subunit of voltage-sensitive calcium channels in the amygdala. *J. Neurochem.* 125, 649-56. <https://doi:10.1111/j.1471-4159.2012.07895.x>.
- Netzahualcoyotzi, C., Tapia, R., 2018. Tetanus toxin C-fragment protects against excitotoxic spinal motoneuron degeneration in vivo. *Sci. Rep.* 8, 16584. <https://doi:10.1038/s41598-018-35027-w>.
- Newman, L.A., Korol, D.L., Gold, P.E., 2011. Lactate produced by glycogenolysis in astrocytes regulates memory processing. *PLoS One.* 6, e28427. <https://doi:10.1371/journal.pone.0028427>.
- Parent, J.M., Yu, T.W., Leibowitz, R.T., Geschwind, D.H., Sloviter, R.S., Lowenstein, D.H., 1997. Dentate granule cell neurogenesis is increased by seizures and contributes to aberrant network reorganization in the adult rat hippocampus. *J. Neurosci.* 17, 3727-38. <https://doi:10.1523/JNEUROSCI.17-10-03727.1997>.
- Pellerin, L., Magistretti, P.J., 1994. Glutamate uptake into astrocytes stimulates aerobic glycolysis: a mechanism coupling neuronal activity to glucose utilization. *Proc. Natl. Acad. Sci. USA.* 91, 10625-10629. <https://doi:10.1073/pnas.91.22.10625>.

- Pierre, K., Chatton, J.Y., Parent, A., Repond, C., Gardoni, F., Di Luca, M., Pellerin, L., 2009. Linking supply to demand: the neuronal monocarboxylate transporter MCT2 and the alpha-amino-3-hydroxyl-5-methyl-4-isoxazole-propionic acid receptor GluR2/3 subunit are associated in a common trafficking process. *Eur. J. Neurosci.* 29, 1951-63. <https://doi:10.1111/j.1460-9568.2009.06756.x>.
- Pierre, K., Pellerin, L., 2005. Monocarboxylate transporters in the central nervous system: distribution, regulation and function. *J. Neurochem.* 94, 1-14. <https://doi.org/10.1111/j.1471-4159.2005.03168.x>.
- Pierre, K., Pellerin, L., Debernardi, R., Riederer, B.M., Magistretti, P.J., 2000. Cell-specific localization of monocarboxylate transporters, MCT1 and MCT2, in the adult mouse brain revealed by double immunohistochemical labeling and confocal microscopy. *Neuroscience.* 100, 617-27. [https://doi.org/10.1016/S0306-4522\(00\)00294-3](https://doi.org/10.1016/S0306-4522(00)00294-3).
- Quintard, H., Patet, C., Zerlauth, J.-B., Suys, T., Bouzat, P., Pellerin, L., Meuli, R., Magistretti, P.J., Oddo, M., 2016. Improvement of neuroenergetics by hypertonic lactate therapy in patients with traumatic brain injury is dependent on baseline cerebral lactate/pyruvate ratio. *J. Neurotrauma.* 33,681-687. <https://doi:10.1089/neu.2015.4057>.
- Robinet, C., Pellerin, L., 2011. Brain-derived neurotrophic factor enhances the hippocampal expression of key postsynaptic proteins in vivo including the monocarboxylate transporter MCT2. *Neuroscience.* 192, 155-63. <https://doi:10.1016/j.neuroscience.2011.06.059>.
- Rosafio, K., Castillo, X., Hirt, L., Pellerin, L., 2016. Cell-specific modulation of monocarboxylate transporter expression contributes to the metabolic reprogramming taking place following cerebral ischemia. *Neuroscience.* 317, 108-20. <https://doi:10.1016/j.neuroscience.2015.12.052>.

- Rosafio, K., Pellerin, L., 2014. Oxygen tension controls the expression of the monocarboxylate transporter MCT4 in cultured mouse cortical astrocytes via a hypoxia-inducible factor-1 α -mediated transcriptional regulation. *Glia*. 62, 477-90. <https://doi:10.1002/glia.22618>.
- Rouach, N., Koulakoff, A., Abudara, V., Willecke, K., Giaume, C., 2008. Astroglial metabolic networks sustain hippocampal synaptic transmission. *Science*. 322(5907):1551-1555. <https://doi:10.1126/science.1164022>.
- Roumes, H., Dumont, U., Sanchez, S., Mazuel, L., Blanc, J., Raffard, G., Chateil, J.-F., Pellerin, L., Bouzier-Sore, A.-K., 2020. Neuroprotective role of lactate in rat neonatal hypoxia-ischemia. *J. Cereb. Blood Flow Metab.* (online ahead of print) <https://doi:10.1177/0271678X20908355>.
- Simpson, I.A., Dwyer, D., Malide, D., Moley, K.H., Travis, A., Vannucci, S.J., 2008. The facilitative glucose transporter GLUT3: 20 years of distinction. *Am. J. Physiol. Endocrinol. Metab.* 295(2):E242-E253. <https://doi:10.1152/ajpendo.90388.2008>.
- Sotelo-Hitschfeld, T., Niemeyer, M. I., Mächler, P., Ruminot, I., Lerchundi, R., Wyss, M. T., Stobart, J., Fernández-Moncada, I., Valdebenito, R., Garrido-Gerter, P., Contreras-Baeza, Y., Schneider, B. L., Aebischer, P., Lengacher, S., San Martín, A., Le Douce, J., Bonvento, G., Magistretti, P. J., Sepúlveda, F. V., Weber, B., Barros, L. F., 2015. Channel-mediated lactate release by K⁺-stimulated astrocytes. *J. Neurosci.* 35(10):4168-4178. <https://doi:10.1523/JNEUROSCI.5036-14.2015>.
- Stone, S.S., Teixeira, C.M., Devito, L.M., Zaslavsky, K., Josselyn, S.A., Lozano, A.M., Frankland, P.W., 2011. Stimulation of entorhinal cortex promotes adult neurogenesis and facilitates spatial memory. *J. Neurosci.* 31, 13469-84. <https://doi:10.1523/JNEUROSCI.3100-11.2011>.

- Strange, B.A., Witter, M.P., Lein, E.S., Moser, E.I., 2014. Functional organization of the hippocampal longitudinal axis. *Nat. Rev. Neurosci.* 15, 655-69. <https://doi:10.1038/nrn3785>.
- Suh, H., Consiglio, A., Ray, J., Sawai, T., D'Amour, K.A., Gage, F.H., 2007. In vivo fate analysis reveals the multipotent and self-renewal capacities of Sox2+ neural stem cells in the adult hippocampus. *Cell Stem Cell.* 1, 515-28. <https://doi:10.1016/j.stem.2007.09.002>.
- Suzuki, A., Stern, S.A., Bozdagi, O., Huntley, G.W., Walker, R.H., Magistretti, P.J., Alberini, C.M., 2011. Astrocyte-neuron lactate transport is required for long-term memory formation. *Cell.* 144, 810-23. <https://doi:10.1016/j.cell.2011.02.018>.
- Tadi, M., Allaman, I., Lengacher, S., Grenningloh, G., Magistretti, P.J., 2015. Learning-induced gene expression in the hippocampus reveals a role of neuron -astrocyte metabolic coupling in long term memory. *PLoS One.* 10, e0141568. <https://doi:10.1371/journal.pone.0141568>.
- van der Staay, F.J., Rutten, K., Erb, C., Blokland, A., 2011. Effects of the cognition impairer MK-801 on learning and memory in mice and rats. *Behav. Brain Res.* 220, 215-29. <https://doi:10.1016/j.bbr.2011.01.052>.
- Vorhees, C.V., Williams, M.T., 2006. Morris water maze: procedures for assessing spatial and related forms of learning and memory. *Nat. Protoc.* 1, 848-858. <https://doi:10.1038/nprot.2006.116>.
- Wang, J., Cui, Y., Yu, Z., Wang, W., Cheng, X., Ji, W., Guo, S., Zhou, Q., Wu, N., Chen, Y., Chen, Y., Song, X., Jiang, H., Wang, Y., Lan, Y., Zhou, B., Mao, L., Li, J., Yang, H., Guo, W., Yang, X., 2019. Brain endothelial cells maintain lactate homeostasis and control adult hippocampal neurogenesis. *Cell Stem Cell.* 25, 754-767.e9. <https://doi:10.1016/j.stem.2019.09.009>.

- Yang J, Ruchti E, Petit JM, Jourdain P, Grenningloh G, Allaman I, Magistretti PJ., 2014. Lactate promotes plasticity gene expression by potentiating NMDA signaling in neurons. *Proc. Natl. Acad. Sci. USA.* 111, 12228-33. [https://doi: 10.1073/pnas.1322912111](https://doi:10.1073/pnas.1322912111).
- Zhang, Y., Chen, K., Sloan, S.A., Bennett, M.L., Scholze, A.R., O'Keefe, S., Phatnani, H.P., Guarnieri, P., Caneda, C., Ruderisch, N., Deng, S., Liddelow, S.A., Zhang, C., Daneman, R., Maniatis, T., Barres, B.A., Wu, J.Q., 2014. An RNA-sequencing transcriptome and splicing database of glia, neurons, and vascular cells of the cerebral cortex. *J. Neurosci.* 34, 11929-47. <https://doi:10.1523/JNEUROSCI.1860-14.2014>.
- Zhou, Z., Liu, A., Xia, S., Leung, C., Qi, J., Meng, Y., Xie, W., Park, P., Collingridge, G.L., Jia, Z., 2018. The C-terminal tails of endogenous GluA1 and GluA2 differentially contribute to hippocampal synaptic plasticity and learning. *Nat. Neurosci.* 21, 50-62. <https://doi:10.1038/s41593-017-0030-z>.
- Zuend, M., Saab, A.S., Wyss, M.T., Ferrari, K.D., Hösli, L., Looser, Z.J., Stobart, J.L., Duran, J., Guinovart, J.J., Barros, L.F., Weber, B., 2020. Arousal-induced cortical activity triggers lactate release from astrocytes. *Nat. Metab.* 2, 179–191. <https://doi.org/10.1038/s42255-020-0170-4>.

Figure legends

Fig. 1. Design for the generation of conditional MCT2 and MCT4 KO mice. (A) Diagram of the MCT2 wild type allele, CKO allele with the loxP sites flanking exon 4 and 5, and the constitutive KO allele after cre recombination. In the right panel, the genotyping results of the corresponding wildtype (WT), heterozygote and homozygote MCT2 floxed mice. The band at 308 bp refers to the WT allele, and the band at 436 bp indicates the loxP insertion. (B) Diagram of the MCT4 WT allele, the CKO allele with the loxP sites flanking exon 3 to 5, and the constitutive KO allele after cre recombination. In the right panel, the genotyping results of the corresponding WT, heterozygote and homozygote MCT4 floxed mice. The band at 388 bp refers to the WT allele, and the band at 516 bp indicates the loxP insertion.

Fig. 2. Cell-specific targeting of neurons or astrocytes in the dorsal hippocampus using AAV-cre viral vectors. Mice were injected into the dorsal hippocampus bilaterally with the adequate AAV vector to target neurons or astrocytes. The diffusion and cell specificity of AAV vectors was evaluated by immunohistochemistry. **(A)** MCT2^{f/f} mice were injected with an AAV-hSyn-GFP-cre and brain sections stained with Hoechst to reveal GFP localization in the anterior, medial, and posterior parts of the hippocampus. **(B)** Colocalization (in yellow) of the reporter protein GFP and the neuronal marker NeuN is shown at high magnification to reveal cell-specificity. Below, quantitative analysis of the percentage of GFP positive cells exhibiting colocalization with the neuronal marker NeuN in different hippocampal subregions. **(C)** MCT4^{f/f} mice were injected with an AAV-GFAP-GFP-cre and sections stained with Hoechst to reveal GFP localization in the anterior, medial, and posterior parts of the hippocampus. **(D)** Colocalization (in yellow) of the reporter protein GFP and the astrocytic protein GFAP is shown at high magnification to reveal cell-specificity. Below, quantitative analysis of the percentage of GFP positive cells exhibiting colocalization with the astrocytic marker GFAP in different hippocampal layers. Data are mean ± s.e.m. (n=4). Scale bars = 200 μm. Pyramidal layer (pyr), granular layer (gr), molecular layer (mo), polymorph layer (polym), *stratum oriens* (or) and *stratum radiatum* (ra).

Fig. 3. Hippocampal expression of the monocarboxylate transporters MCT1 (*Slc16a1*), MCT2 (*Slc16a7*) and MCT4 (*Slc16a3*) following reduced expression levels of either MCT2 in neurons or MCT4 in astrocytes. Expression levels have been evaluated by quantitative analysis of mRNA and protein levels in dorsal hippocampal extracts. **(A,B)**, mRNA levels following reduced expression levels of MCT2 in neurons **(A)** or MCT4 in astrocytes **(B)** were determined by RT-qPCR. Expression levels were normalized with *YWHAZ* (tyrosine 3-

monooxygenase/tryptophan 5-monooxygenase activation protein zeta). **(C,D)** Illustrative western blots of hippocampal MCT1, MCT2 and MCT4 protein expression following reduced expression levels of MCT2 in neurons **(C)** or MCT4 in astrocytes **(D)**. **(E,F)**, Densitometric analysis of western blots for MCT expression following reduced expression levels of MCT2 in neurons **(E)** or MCT4 in astrocytes **(F)**. Protein levels were normalized with β -tubulin. Data are mean \pm s.e.m. (n=5-6), two-sample *t*-test (ctrl vs. cre, details in Supplementary Table 1). Only significant P values are reported.

Fig. 4. Short-term (90-min) and long-term (24-h) memory in mice with reduced expression levels of neuronal MCT2 or astrocytic MCT4 in the hippocampus. **(A)** Diagram summarizing the experimental procedure. Three weeks after the appropriate AAV injection, mice were evaluated in two distinct behavioral tasks with a protocol composed of one day of training trial(s), followed by an interval of 90 min or 24 h before the probe trial. **(B)** IA test: the latency to cross to the dark chamber was measured 24 h after the training trial. **(C)** NOR test: recognition indexes measured during training (left panel) and probe trials (right panel) when the interval between these sessions was 90 min. **(D)** NOR test: recognition indexes measured during training (left panel) and probe trials (right panel) when the interval between these sessions was 24 h. Data are mean \pm s.e.m. (n=5-7). Statistical analyses: **(B,D)** two-sample *t*-test (ctrl vs. cre, details in Supplementary Table 1). When statistically significant, P value is shown. In **(C,D)** one-sample *t*-test vs. chance level (0.5).

Fig. 5. Acquisition and consolidation of spatial information in mice with reduced expression levels of neuronal MCT2 or astrocytic MCT4 in the hippocampus. **(A)** Diagram

summarizing the experimental procedure. Three weeks after the appropriate AAV injection, mice were trained during 6 days (4 trials/day) in the MWM, and underwent a probe trial after a 7-day interval. Some mice were i.c.v. infused during the training period with L-lactate (LAC) or vehicle (veh). **(B)** Extracellular LAC levels measured using microdialysis in the dorsal hippocampus of freely moving sham MCT2^{f/f} mice with or without LAC infusion. **(C)** Training for MCT2^{f/f} mice with (cre) or without (ctrl) reduced neuronal MCT2 expression levels and with or without LAC infusion. Average time to reach the platform on each training day. **(D)** Probe test for MCT2^{f/f} mice. Percentage of time spent in the TQ. **(E)** Representative heatmaps of cumulative trajectories during the probe trial for MCT2^{f/f} mice with (cre) or without (ctrl) reduced neuronal MCT2 expression levels. **(F)** Training for MCT4^{f/f} mice with (cre) or without (ctrl) reduced astrocytic MCT4 expression levels and with or without LAC infusion. Average time to reach the platform on each training day. **(G)** Probe test for MCT4^{f/f} mice. Percentage of time spent in the TQ. **(H)** Representative heatmaps of cumulative trajectories during the probe trial for MCT4^{f/f} mice with (cre) or without (ctrl) reduced astrocytic MCT4 expression levels. Data are mean \pm s.e.m. (n=4 for **B** and n=6-8 for the others). Statistical analyses: **(B)** two-sample *t*-test. (veh vs LAC, details in Supplementary Table 1). **(C,F)** two-way ANOVA and Tukey's post-hoc test. Significant P values vs ctrl* and vs LAC[#] group (more details in Supplementary Table 2). **(D,G)** Kruskal-Wallis followed by Dunns's test. Only significant P values are reported.

Fig. 6. Neurogenesis and neurodegeneration in mice with reduced expression levels of neuronal MCT2 or astrocytic MCT4 in the hippocampus. **(A)** Representative images of Sox2 immunohistochemistry in the dorsal DG of coronal brain sections from mice that completed the MWM protocol or sham animals (non-injected MCT2^{f/f} mice with no behavioral

evaluation) (top row). When an AAV was injected, the GFP reporter protein labeling is also shown in the merge pictures of the bottom row. We included nuclear labeling with Hoechst to provide a reference location. **(B)** Quantitative analysis of Sox2⁺ cells in the SGZ of the DG. **(C)** Representative pictures of DCX immunohistochemistry in the medial dorsal hippocampus (top row) and the corresponding magnifications (bottom row) in coronal brain sections from mice three weeks after AAV injection or sham animals (non-injected MCT2^{f/f} mice). When an AAV was injected, the GFP reporter protein labeling indicates the cell specificity of infection (middle row). **(D)** Quantitative analysis of DCX staining in the DG. Three histological sections/mouse were analyzed. **(E)** Representative pictures of silver staining in the dorsal DG. Dark brown or black areas are silver deposits indicating degeneration (arrows). The positive control for neurodegeneration was obtained by injection of 1 μ l of AMPA at 0.01 mM in the hippocampus of a sham MCT2^{f/f} mouse. Data are mean \pm s.e.m. (n=8-12). Statistical analyses: **(B,D)** Two-sample *t*-test (ctrl vs. cre, details in Supplementary Table 1). When statistically significant, P value is shown. Scale bars = 50 μ m.

Supplementary Fig. 1. Expression analysis of specific genes of interest in the hippocampus after reduced expression levels of either neuronal MCT2 or astrocytic MCT4. **(A)** mRNA expression levels of different glucose transporters and glutamate receptor subunits in the hippocampus of floxed mice with (cre) or without (ctrl) reduced neuronal MCT2 expression levels. **(B)** mRNA expression levels of different glucose transporters and glutamate receptor subunits in the hippocampus of floxed mice with (cre) or without (ctrl) reduced astrocytic MCT4 expression levels. **(C)** mRNA and protein expression levels of the AMPA receptor subunit GluA2 in the hippocampus of floxed mice with (cre) or without (ctrl) reduced neuronal MCT2 expression levels or **(D)** with (cre) or without (ctrl) reduced astrocytic MCT4 expression

levels. mRNA expression levels were normalized with *YWHAZ*. Protein levels were normalized with β -tubulin. Correspondence between gene abbreviation and protein description: *Slc2a1* (GLUT1, glucose transporter type 1), *Sl2a3* (GLU3, glucose transporter type 3), *Gria1* (GluA1, glutamate receptor AMPA-type subunit 1), *Gria2* (GluA2, glutamate receptor AMPA-type subunit 2), *Grin 1* (GluN1, glutamate receptor NMDA-type subunit 1) and *Grin2* (GluN2, glutamate receptor NMDA-type subunit 2). Data are mean \pm s.e.m. (n=5-8), two-sample *t*-test (ctrl vs. cre, details in Supplementary Table 1). When statistically significant, P value is shown.

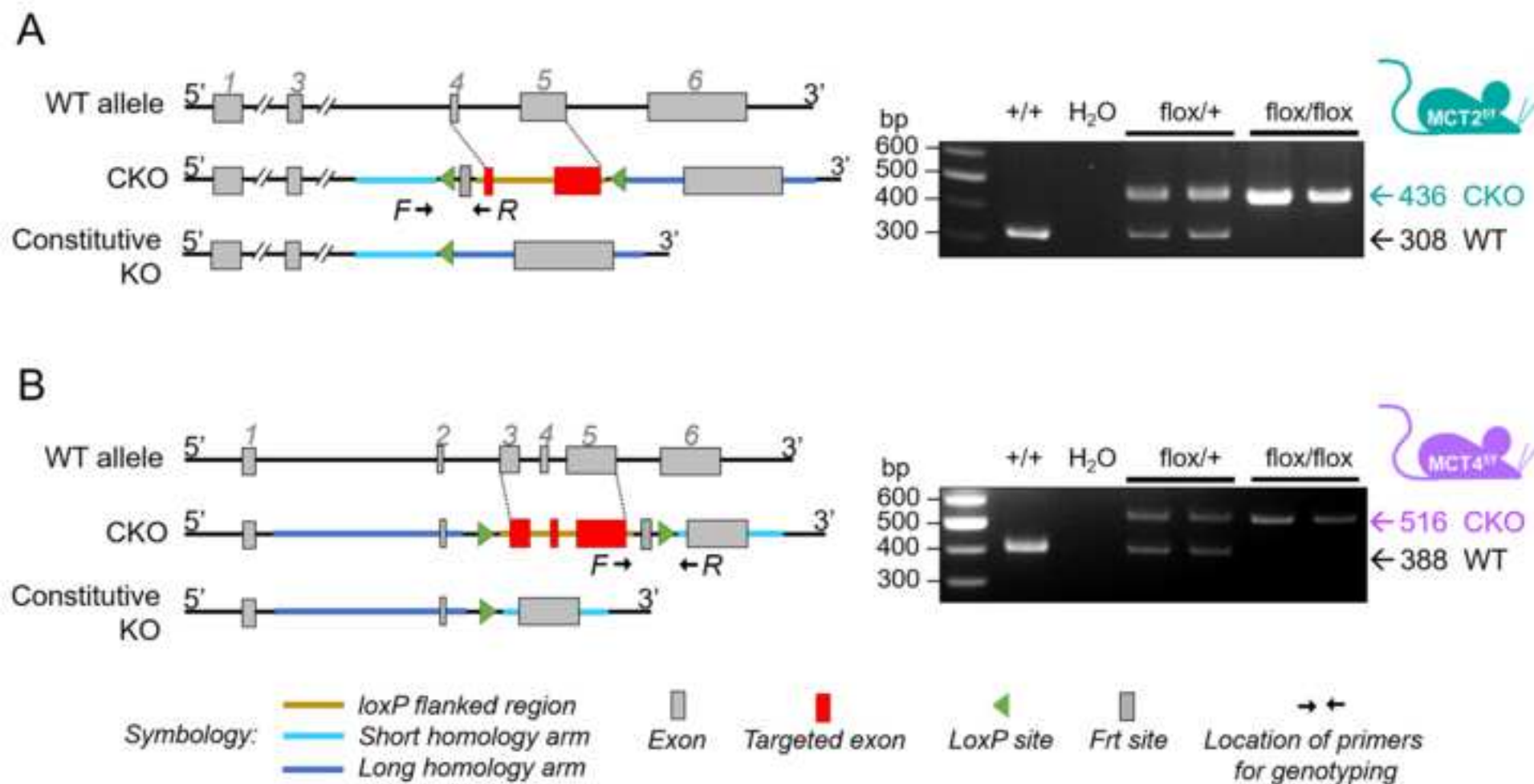
Supplementary Fig. 2. Behavioral performances of sham MCT2^{f/f} and MCT4^{f/f} mice. (A)

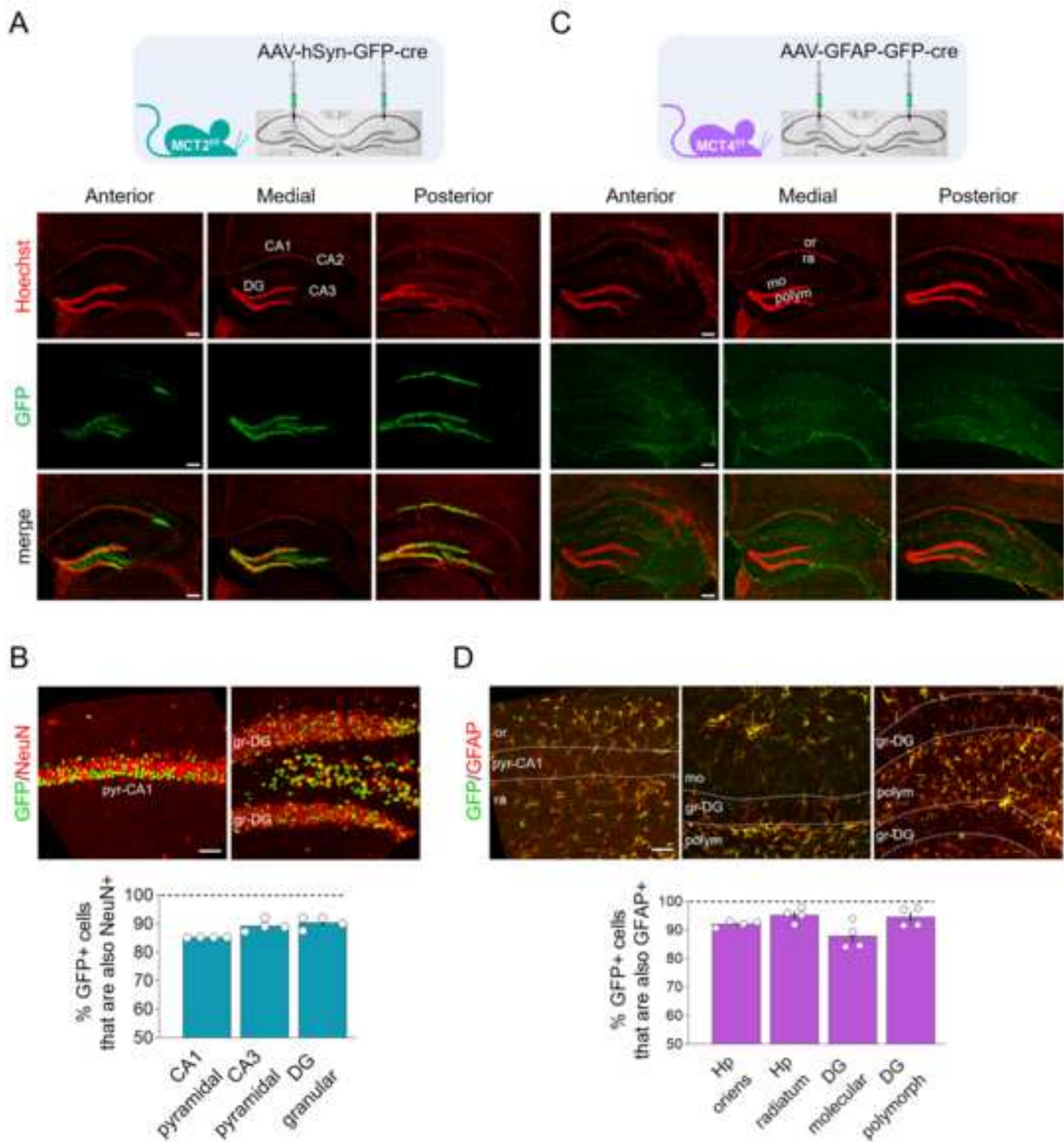
Motor performance as evaluated by measuring walking (upper panel) and swimming (lower panel) speed. **(B)** 90-min (upper row) and 24-h (lower row) memory as determined with the NOR test. Left panels represent recognition indexes for training with two identical objects (Training). Right panels (Probe test) represent recognition indexes after the introduction of the novel object with a certain delay after training. **(C)** Learning and 7-days long-term memory was evaluated with the MWM task. Left panel presents the average time to reach the platform on each training day. Right panel presents the percentage of time spent in the TQ. Bottom panel shows representative heatmap of cumulative trajectories/group at the probe trial. A group of WT mice which received an i.p. administration (0.1 mg/kg) of the noncompetitive antagonist of the N-Methyl-D-aspartate receptor, MK-801, 30 min before the beginning of each training session, was used as a positive control of cognitive impairment in all behavioral tasks. Data are mean \pm s.e.m. (n=4-10). Statistical analyses: **(A)** one-way ANOVA. **(B)** one-sample *t*-test vs. chance level (0.5) and *t*-test. **(C)** two-way ANOVA and Tukey's post-hoc test (left side). Significant P values vs the other groups* (more details in Supplementary Table 2). One-way ANOVA (right side).

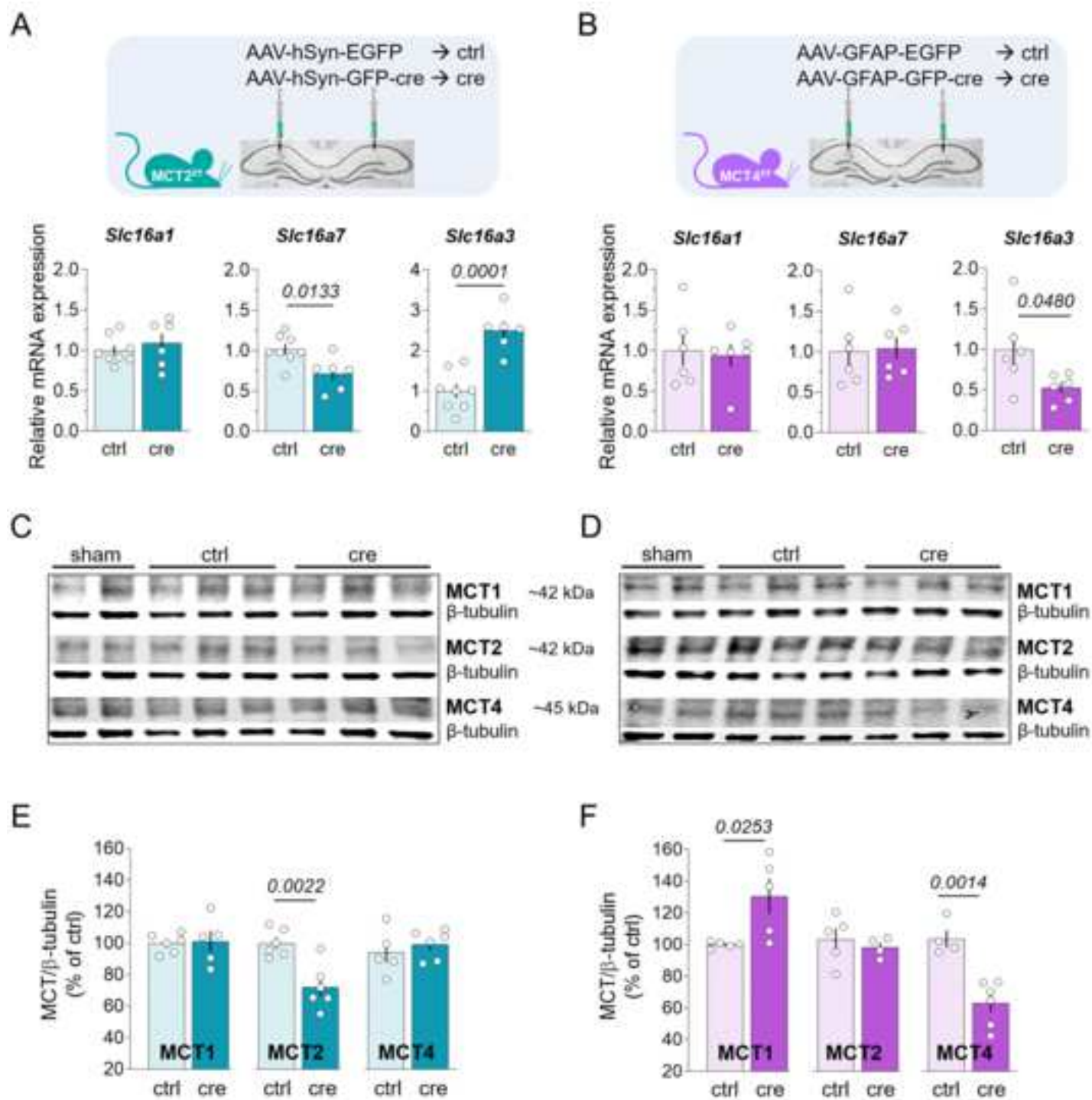
Supplementary Fig. 3. Behavioral assessment of anxiety, innate fear, motivational behavior and working memory in mice with reduced expression levels of neuronal MCT2 or astrocytic MCT4 in the hippocampus. (A) Three weeks after the appropriate AAV injection, mice were tested in different behavioral tasks to assess the following parameters. (B) Walking speed (left panel) and thigmotaxis (right panel) measured in the open field paradigm. (C) Time in closed arms of the elevated plus-maze. (D) Immobility time when exposed to vehicle (left, veh) and trimethylthiazoline (right panel, TMT) as part of the odor predator test. (E) Activity parameters registered in the forced swimming test. (F) Spontaneous alternation in the Y-maze test. Data are mean \pm s.e.m. (n=6-8), two-sample *t*-test (ctrl vs. cre, details in Supplementary Table 1). When statistically significant, P value is shown except for the Y-maze test with P values that did not reach significance (ns).

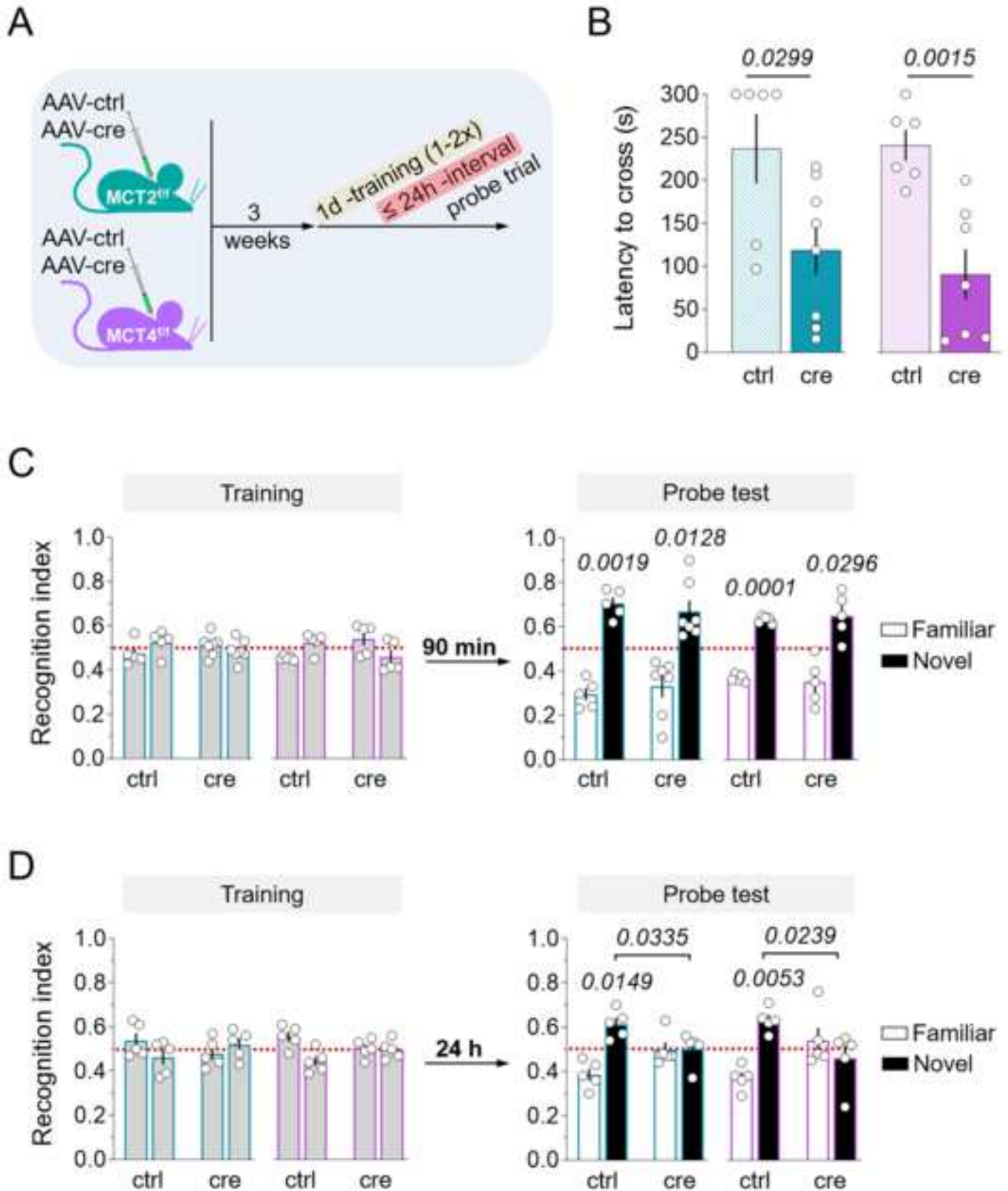
Supplementary Fig. 4. Effect of glucose i.c.v. infusion on acquisition and consolidation of spatial information in mice with reduced expression levels of neuronal MCT2 or astrocytic MCT4 in the hippocampus. (A) Training of MCT2^{f/f} mice with (cre) reduced neuronal MCT2 expression levels and with glucose infusion. Average time to reach the platform on each training day. (B) Percentage of time spent in the TQ during the probe test. The reference curves and columns shown in color are the expected mean values for ctrl and cre groups as reported in Fig. 5C and 5D. (C) Training of MCT4^{f/f} mice with (cre) reduced astrocytic MCT4 expression levels and with glucose infusion. Average time to reach the platform on each training day. (G) Percentage of time spent in the TQ during the probe test. The reference curves and columns shown in color are the expected mean values for ctrl and cre groups as reported in Fig. 5F and 5G.

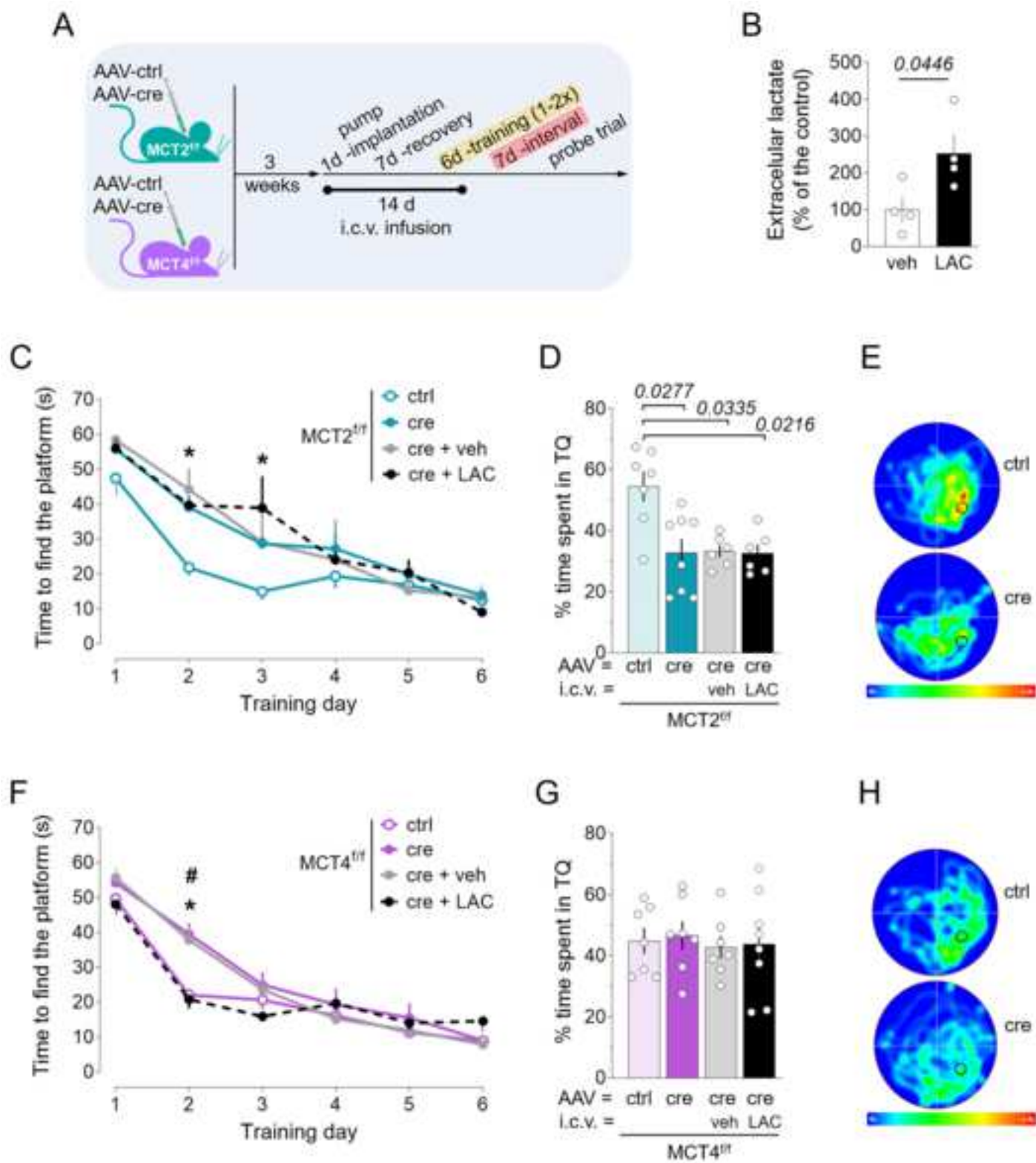
Supplementary Fig. 5. Effect of the AMPA receptor GluA2 subunit antagonist Perampanel on the acquisition and consolidation of spatial information as well as on neurogenesis. MCT2^{f/f} mice were i.c.v. infused with the GluA2 subunit inhibitor Perampanel (PER), or vehicle (veh) during the training period of 6 days (4 trials/day) and memory probe trial of the MWM test. **(A)** Training for MCT2^{f/f} mice with or without i.c.v. PER infusion. Average time to reach the platform on each training day. Ctrl and cre groups are the same ones reported in Fig. 5C. **(B)** Probe test for MCT2^{f/f} mice with or without i.c.v. PER infusion. Percentage of time spent in the TQ. Ctrl and cre groups are the same ones reported in Fig. 5D. **(C)** Representative pictures DCX immunohistochemistry in the medial dorsal DG (top row) and the corresponding magnifications (middle row) in coronal brain sections from mice i.c.v. infused with PER and that completed the MWM test. At the bottom, a representative picture of silver staining in the same region with no sign of degeneration. **(D)** Quantitative analysis of DCX staining in the DG. Sham, ctrl and cre groups are the same ones reported in Fig. 6D. Three histological sections/mouse were analyzed. Data are mean \pm s.e.m. (n=7-12). Statistical analyses: **(A)** Two-way ANOVA and Tukey's post-hoc test. Significant P values ctrl vs cre* as reported before, and ctrl vs PER[#] (more details in Supplementary Table 2). **(B, D)** One-way ANOVA. Significant P values are shown, ctrl vs cre* as reported before. Scale bars = 50 μ m.

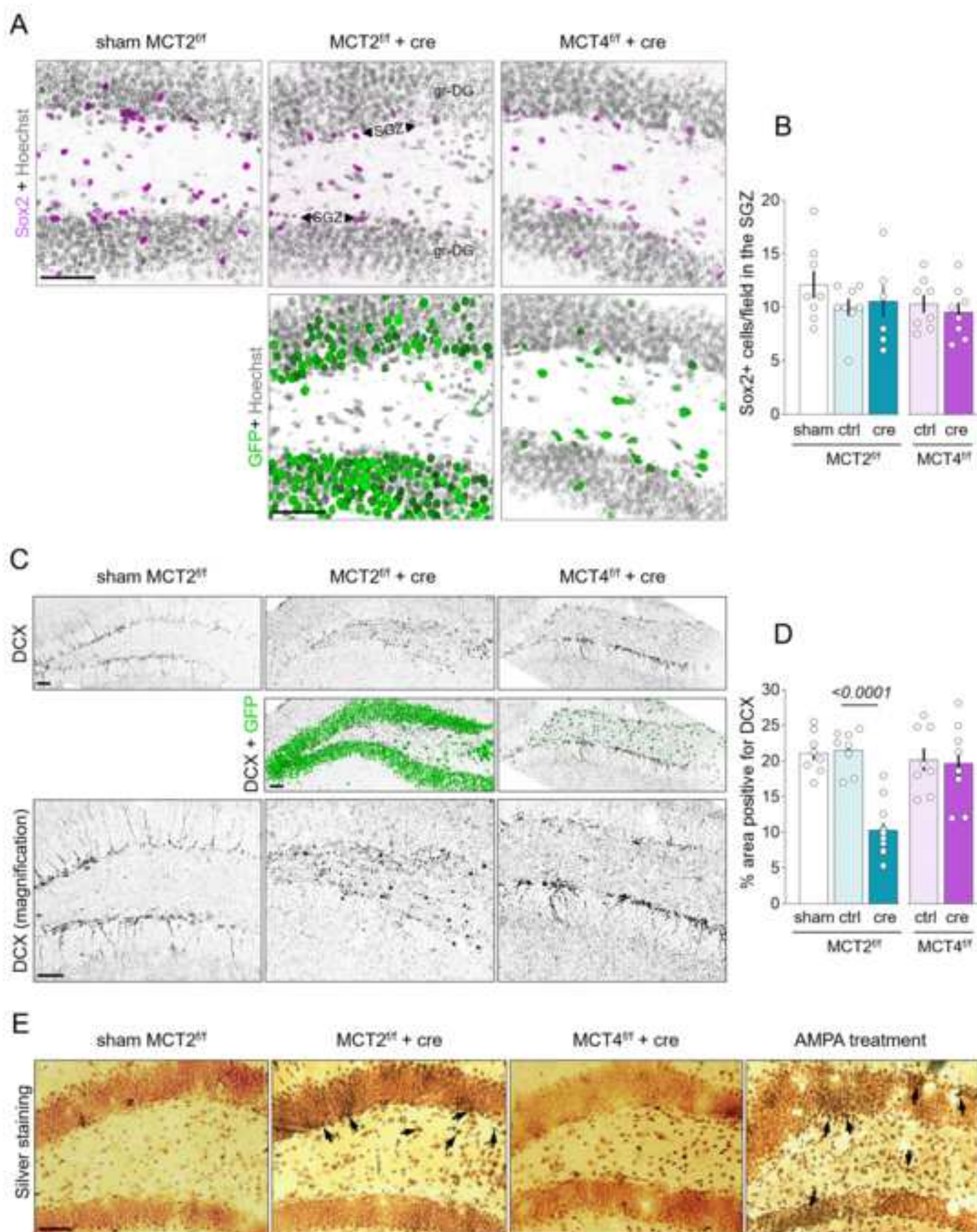














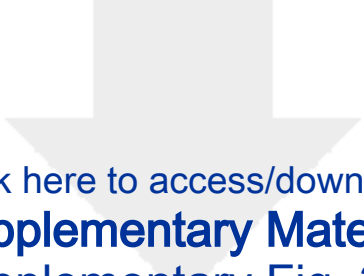
Click here to access/download
Supplementary Material
Supplementary Fig. 1.tif






Click here to access/download
Supplementary Material
Supplementary Fig. 2.tif





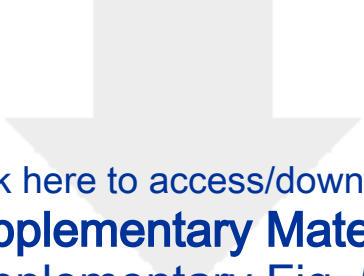
Click here to access/download
Supplementary Material
Supplementary Fig. 3.tif





Click here to access/download
Supplementary Material
Supplementary Fig. 4.tif





Click here to access/download
Supplementary Material
Supplementary Fig. 5.tif

